

This is a repository copy of *An Operationally Unsaturated Iridium-Pincer Complex That C-H Activates Methane and Ethane in the Crystalline Solid-State*.

White Rose Research Online URL for this paper:

<https://eprints.whiterose.ac.uk/223001/>

Version: Published Version

---

**Article:**

Weller, Andrew [orcid.org/0000-0003-1646-8081](https://orcid.org/0000-0003-1646-8081), Gyton, Matthew Robert [orcid.org/0000-0002-7565-5154](https://orcid.org/0000-0002-7565-5154), Johnson, Chloe-Louise et al. (2 more authors) (2025) An Operationally Unsaturated Iridium-Pincer Complex That C-H Activates Methane and Ethane in the Crystalline Solid-State. *Journal of the American Chemical Society*. ISSN 1520-5126

<https://doi.org/10.1021/jacs.4c18122>

---

**Reuse**

This article is distributed under the terms of the Creative Commons Attribution (CC BY) licence. This licence allows you to distribute, remix, tweak, and build upon the work, even commercially, as long as you credit the authors for the original work. More information and the full terms of the licence here:

<https://creativecommons.org/licenses/>

**Takedown**

If you consider content in White Rose Research Online to be in breach of UK law, please notify us by emailing [eprints@whiterose.ac.uk](mailto:eprints@whiterose.ac.uk) including the URL of the record and the reason for the withdrawal request.

# An Operationally Unsaturated Iridium-Pincer Complex That C–H Activates Methane and Ethane in the Crystalline Solid-State

Matthew R. Gyton, M. Arif Sajjad, Daniel J. Storm, Kristof M. Altus, Joe C. Goodall, Chloe L. Johnson, Samuel J. Page, Alison J. Edwards, Ross O. Piltz, Simon B. Duckett, Stuart A. Macgregor,\* and Andrew S. Weller\*



Cite This: <https://doi.org/10.1021/jacs.4c18122>



Read Online

ACCESS |



Metrics & More



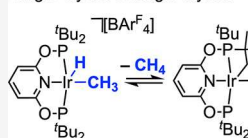
Article Recommendations



Supporting Information

**ABSTRACT:** The known complex  $[\text{Ir}(\text{}^t\text{Bu-PONOP})\text{MeH}][\text{BAR}^{\text{F}}_4]$ , **1** [ $\text{BAR}^{\text{F}}_4$ ] [ $\text{}^t\text{Bu-PONOP} = \kappa^3\text{-}2,6\text{-}(\text{}^t\text{Bu}_2\text{PO})_2\text{C}_5\text{H}_3\text{N}$ ;  $\text{Ar}^{\text{F}} = 3,5\text{-}(\text{CF}_3)_2(\text{C}_6\text{H}_3)$ ; *J. Am. Chem. Soc.* **2009**, 131, 8603], is a robust precursor for *in crystallo* single-crystal to single-crystal (SC-SC) C–H activation of methane and ethane at 80 °C. This contrasts with the reported solution ( $\text{CD}_2\text{Cl}_2$ ) behavior, where **1** [ $\text{BAR}^{\text{F}}_4$ ] decomposes by methane loss. Crystalline **1** [ $\text{BAR}^{\text{F}}_4$ ] is accessed as a single polymorph on a gram scale. A single-crystal neutron diffraction study locates the hydride.  $^{13}\text{C}\{^1\text{H}\}$  SSNMR experiments on **1** [ $\text{BAR}^{\text{F}}_4$ ], and its isotopologue  $[\text{Ir}(\text{}^t\text{Bu-PONOP})(\text{CD}_3\text{D})][\text{BAR}^{\text{F}}_4]$ , **d**<sub>4</sub>-**1** [ $\text{BAR}^{\text{F}}_4$ ], suggest a rapid and reversible endergonic reductive bond formation is occurring *in crystallo* to access an Ir(I)  $\sigma$ -methane complex. Heating **1** [ $\text{BAR}^{\text{F}}_4$ ] to 80 °C under high vacuum results in loss of methane and intramolecular C–H activation to form cyclometalated  $[\text{Ir}(\text{cyclo-}^t\text{Bu-PONOP}')\text{H}][\text{BAR}^{\text{F}}_4]$ , **2** [ $\text{BAR}^{\text{F}}_4$ ], in a SC-SC reaction. This is reversible, and the addition of  $\text{CH}_4$  or  $\text{CD}_4$  to **2** [ $\text{BAR}^{\text{F}}_4$ ] at 80 °C results in an equilibrium with **1** [ $\text{BAR}^{\text{F}}_4$ ] or **d**<sub>4</sub>-**1** [ $\text{BAR}^{\text{F}}_4$ ], respectively. Complex **2** [ $\text{BAR}^{\text{F}}_4$ ] is thus an operationally unsaturated source of 14-electron  $[\text{Ir}(\text{}^t\text{Bu-PONOP})][\text{BAR}^{\text{F}}_4]$ , **III**, that undergoes C–H activation with methane. Periodic DFT studies, alongside isotope labeling experiments, link **1** [ $\text{BAR}^{\text{F}}_4$ ] and **2** [ $\text{BAR}^{\text{F}}_4$ ]/ $\text{CH}_4$  via a reductive elimination/oxidative addition pathway. Heating **2** [ $\text{BAR}^{\text{F}}_4$ ] to 80 °C under  $\text{N}_2$  forms  $[\text{Ir}(\text{}^t\text{Bu-PONOP})(\kappa^1\text{-N}_2)][\text{BAR}^{\text{F}}_4]$ , in a SC-SC transformation. Reaction with CO forms  $[\text{Ir}(\text{}^t\text{Bu-PONOP})(\text{CO})][\text{BAR}^{\text{F}}_4]$  at room temperature. Calculations suggest reaction with  $\text{N}_2$  occurs via an associative process or competitively through **III**, while with CO only an associative process operates. Heating **2** [ $\text{BAR}^{\text{F}}_4$ ] to 80 °C under an ethane atmosphere results in alkane dehydrogenation, via a SC–SC reaction, forming a ~1:1 mixture of  $[\text{Ir}(\text{}^t\text{Bu-PONOP})(\eta^2\text{-H}_2\text{C}=\text{CH}_2)][\text{BAR}^{\text{F}}_4]$ , and  $[\text{Ir}(\text{}^t\text{Bu-PONOP})\text{H}_2][\text{BAR}^{\text{F}}_4]$ .

*In crystallo* C–H activation  
Single-crystal to single-crystal



- \* SC-SC reactivity
- \* H/D isotope effects
- \* Methane C–H activation
- \* Ethane dehydrogenation
- \* Periodic DFT

## INTRODUCTION

The coordination and activation of methane in molecular metal/ligand complexes has been a grand-challenge in organometallic chemistry<sup>1–7</sup> since the report by Shilov in the early 1970s of homogeneous platinum-based systems that convert methane to methanol.<sup>8</sup> The interest in methane activation comes from the abundance of this C<sub>1</sub> feedstock and opportunities for upgrading into more valuable chemicals or energy vectors.<sup>9,10</sup> While heterogeneous catalysis offers promise for methane valorization on an industrial scale,<sup>11,12</sup> doing so selectively, efficiently and under relatively mild conditions represents a significant challenge, as the C–H bond in methane is strong (homolytic bond strength = 105 kcal/mol,<sup>13</sup> nonpolar and sterically hindered (sp<sup>3</sup> carbon). Nevertheless elegant examples of catalytic methane activation using homogeneous molecular organometallic complexes have been reported.<sup>1,14–21</sup> Several mechanisms for the C–H bond activation of methane have been established, and include outer-sphere processes (e.g., in metalloenzymes or iron-oxo complexes<sup>22</sup>) or  $\sigma$ -bond metathesis.<sup>23</sup> Mechanisms based on inner-sphere coordination of the C–H bond to form an

intermediate  $\sigma$ -methane complex,<sup>24</sup> with a 3c–2e M...H–C bond,<sup>25</sup> result in activation by oxidative cleavage or  $\sigma$ -complex assisted metathesis.<sup>26,27</sup> The role of reactive unsaturated intermediates that are primed for coordination of methane to form intermediate  $\sigma$ -complexes are thus important in its C–H activation.

Despite this considerable interest, the observation of precursor methane  $\sigma$ -complexes,<sup>7,28–32</sup> Figure 1A, or the direct products of methane C–H activation,<sup>2,33–40</sup> exemplified in Figure 1B,<sup>41</sup> are still relatively rare, as the weak binding of methane, and alkanes more generally<sup>6,7,24,27</sup>, to metal centers results in competition with solvent or a displaced ligand, such as photochemically generated CO. Consequently,  $\sigma$ -methane complexes are short-lived and have only been characterized *in*

Received: December 18, 2024

Revised: February 3, 2025

Accepted: February 6, 2025

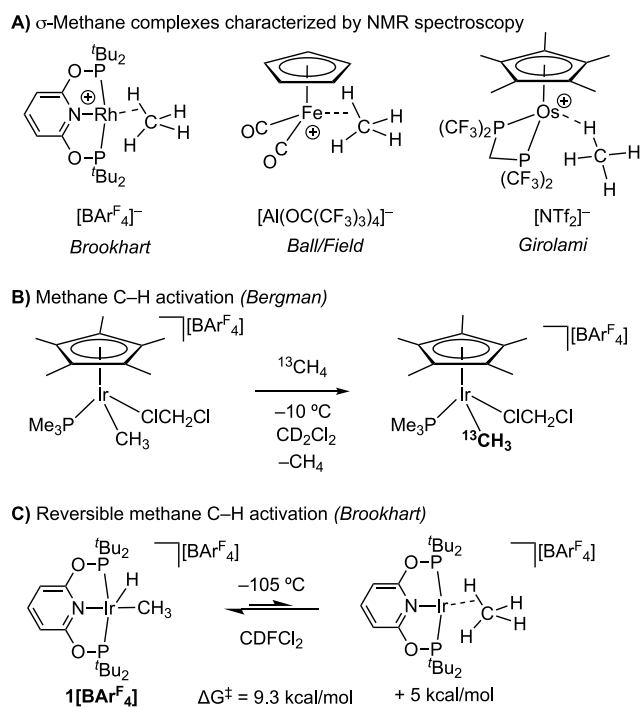


**Figure 1.** Methane  $\sigma$ -complexes and C–H activation.

*situ* at low temperatures by matrix isolation methods, or in solutions of weakly binding solvents, using NMR or time-resolved infrared spectroscopy. These conditions also mean that a structural analysis of a  $\sigma$ -methane complex using single-crystal X-ray diffraction has not yet been realized, although *in situ* neutron powder diffraction experiments on methane uptake in MOF-type materials show metal $\cdots\text{H}_4\text{C}$  interactions, albeit weak.<sup>42,43</sup> In addition, as the thermodynamics of methane C–H activation are finely balanced, the position of the dynamic equilibrium between a  $\sigma$ -complex and its tautomeric methyl hydride can be influenced by the identity of the metal center and ligand choice.<sup>28,44–47</sup> Of direct relevance to this work is the example from Brookhart and coworkers of an Ir(III) methyl hydride complex  $[\text{Ir}(\text{tBu-PONOP})\text{MeH}][\text{BAR}^{\text{F}}_4]$ , **1** $[\text{BAR}^{\text{F}}_4]$ ,<sup>48</sup> that is in rapid exchange with the corresponding, higher energy, Ir(I)  $\sigma$ -methane complex  $[\text{Ir}(\text{tBu-PONOP})(\text{H}_4\text{C})][\text{BAR}^{\text{F}}_4]$  at  $-105\text{ }^\circ\text{C}$  in  $\text{CDCl}_2\text{F}$  solution, **Figure 1C** [ $\text{tBu-PONOP} = \kappa^3\text{-2,6-(tBu}_2\text{PO)}_2\text{C}_5\text{H}_3\text{N}$ ;  $\text{Ar}^{\text{F}} = 3,5\text{-(CF}_3)_2\text{C}_6\text{H}_3$ ].

We have been developing solid/gas single-crystal to single-crystal<sup>49–51</sup> (SC-SC) *in crystallo*<sup>52</sup> reactivity to synthesize remarkably stable, compared with *in situ* solution methods,  $\sigma$ -alkane complexes by addition of excess  $\text{H}_2$  to precursor alkene complexes.<sup>53</sup> We refer to this approach as solid-state molecular organometallic chemistry, SMOM,<sup>54</sup> that is related to, but distinct from, surface organometallic chemistry, SOMC,<sup>55</sup> where highly active organometallic complexes are grafted onto a platform support. The prototypical SMOM example is the addition of  $\text{H}_2$  to single-crystals of the cationic Rh(I) complex  $[\text{Rh}(\text{Cy}_2\text{PCH}_2\text{CH}_2\text{PCy}_2)(\text{NBD})][\text{BAR}^{\text{F}}_4]$  (NBD = norbornadiene). This results in rapid double-bond hydrogenation and formation of the corresponding room temperature stable  $\sigma$ -alkane complex,  $[\text{Rh}(\text{Cy}_2\text{PCH}_2\text{CH}_2\text{PCy}_2)(\text{NBA})][\text{BAR}^{\text{F}}_4]$  **I** (NBA = norbornane), that can be characterized by single-crystal X-ray and neutron diffraction, solid-state NMR spectroscopy and periodic DFT calculations, **Figure 2A**.<sup>56–58</sup>

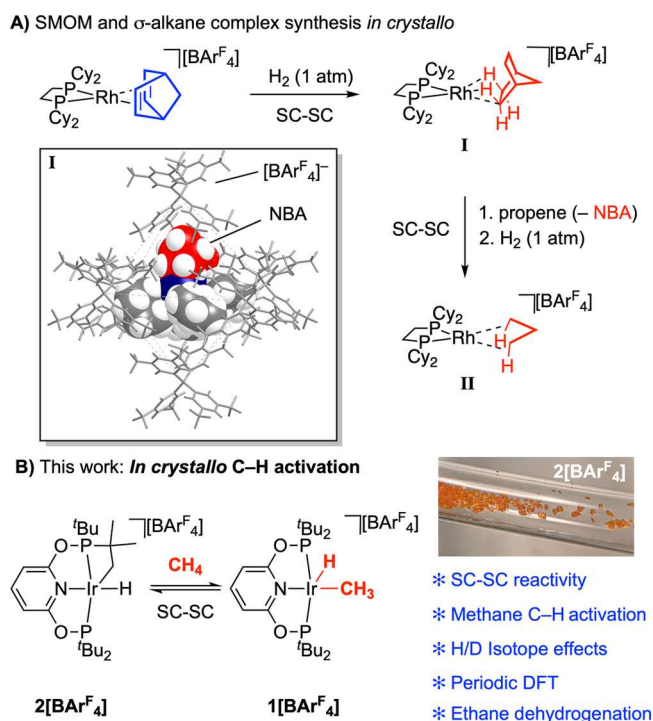


**Figure 2.** (A) *In crystallo* SMOM and  $\sigma$ -alkane complexes. Cation shown at van der Waals radii. (B) This work. SC-SC = single-crystal to single-crystal.

With solvent absent, and any competitive pre-equilibria for alkane binding removed, such  $\sigma$ -alkane complexes have been shown to undergo room temperature intramolecular C–H activation *in crystallo*, for example selective H/D exchange at bound NBA or cyclohexane with  $\text{D}_2$ <sup>58,59</sup> or alkane dehydrogenation of bound cyclohexane.<sup>59</sup> The stability in the solid-state comes from the absence of solvent combined with the secondary microenvironment provided by a cage of  $[\text{BAR}^{\text{F}}_4]^-$  anions that encapsulate the cationic  $\sigma$ -alkane complex, in which noncovalent interactions with the alkane (directional C–F $\cdots\text{H}$ –C and more diffuse C–H $\cdots\pi$ ) play an important role.<sup>57,60–62</sup> These anions, with their  $\text{CF}_3$  groups, also allow for substrate ingress and product egress through the nonporous crystalline lattice.<sup>63</sup> For example, **I** reacts with propene to displace the bound NBA ligand in a SC-SC transformation to form the corresponding propene complex,<sup>54</sup> which can then undergo further SC-SC reaction with  $\text{H}_2$  to form the corresponding (albeit short-lived) crystallographically characterized  $\sigma$ -propane complex, **II**.<sup>60</sup>

The intermolecular coordination and activation of methane is, however, challenging using this SMOM ligand exchange approach. First, the pseudodegenerate exchange of a relatively strongly<sup>57,60</sup> encapsulated alkane ligand (i.e.,  $\eta^2\eta^2$ -NBA) for methane is likely to be both thermodynamically disfavored and kinetically slow. Second, while *in crystallo* hydrogenolysis of a suitable precursor, such as a methylidene complex,<sup>64</sup> would form methane, this would rapidly be displaced by  $\text{H}_2$  under the conditions of excess  $\text{H}_2$ ,<sup>45,65</sup> and is further complicated by the local concentration of  $\text{H}_2$  in a single-crystal being modified by spatial and temporal constraints.<sup>66–69</sup> We now report an alternative approach for the straightforward coordination and activation of methane in a SC-SC process using a molecular organometallic complex, **Figure 2B**. The *in crystallo* synthesis of an “operationally unsaturated”<sup>70–72</sup> cyclometalated Ir(III)-

hydride pincer complex,  $2[\text{BAR}^{\text{F}}_4]$ , allows for C–H activation of methane at a reactive Ir(I) center to form the corresponding methyl hydride,  $1[\text{BAR}^{\text{F}}_4]$ ,<sup>48</sup> under mild conditions (80 °C, up to 8 bar  $\text{CH}_4$ ). This reaction is reversible while retaining single crystallinity, and light alkane activation can be extended to the dehydrogenation of ethane. The generation of unsaturated 14-electron Ir(I)-pincer complexes that undergo C–H activation is of direct relevance to alkane-dehydrogenation catalysis where such intermediates are postulated.<sup>73,74</sup>

## RESULTS AND DISCUSSION

**Isolation of Room Temperature Stable  $[\text{Ir}(\text{tBu-PONOP})\text{MeH}][\text{BAR}^{\text{F}}_4]$ ,  $1[\text{BAR}^{\text{F}}_4]$ , as Single Crystals on Gram Scale: Polymorphs and Structural Characterization Using Single-Crystal Neutron Diffraction.** To generate an operationally unsaturated complex using *in crystallo* methods we chose Brookhart's  $[\text{Ir}(\text{tBu-PONOP})\text{MeH}][\text{BAR}^{\text{F}}_4]$ ,  $1[\text{BAR}^{\text{F}}_4]$ , as its low temperature recrystallization (−35 °C) on the 20–30 mg scale, and structural characterization using single-crystal X-ray diffraction, have been reported.<sup>48</sup>  $1[\text{BAR}^{\text{F}}_4]$  is unstable in solution, losing methane via reductive elimination at 29 °C [ $t_{1/2}$  = 3 h]. The organometallic products of methane loss were not described, although for related systems binding of solvent has been proposed<sup>46</sup> or observed.<sup>29,75</sup> We speculated that *in crystallo* loss of methane from  $1[\text{BAR}^{\text{F}}_4]$ , in the absence of solvent, would result in a reactive low coordinate species that could then undergo further C–H activation processes with gaseous alkanes. In support of this approach, we and others, have shown that pincer-ligand motifs can support single-crystal to single-crystal solid/gas reactivity.<sup>64,76–79</sup>

Using a slightly revised preparation,  $1[\text{BAR}^{\text{F}}_4]$  was synthesized and isolated by slow (weeks) low temperature recrystallization at −40 °C ( $1,2\text{-F}_2\text{C}_6\text{H}_4/\text{heptane}$ ) to repeatedly afford orange blocks in greater than 90% isolated yield on a 1.1–1.4 g scale, Figure 3A. In contrast to its instability in solution, under an argon atmosphere at ambient temperatures crystalline  $1[\text{BAR}^{\text{F}}_4]$  is stable for months, as shown by low

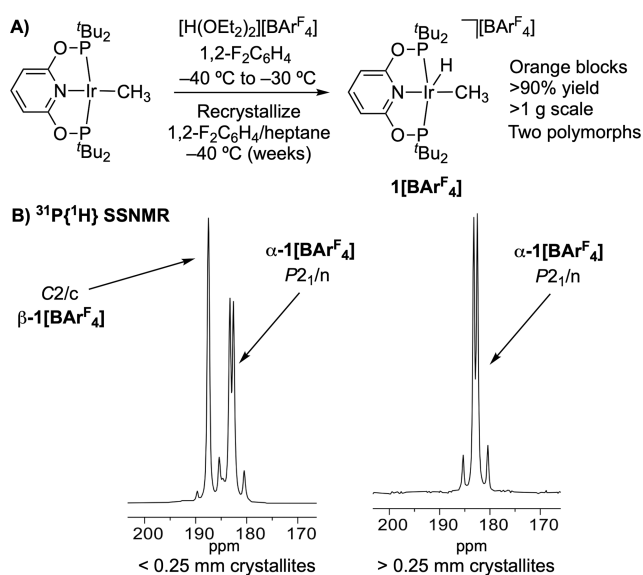


**Figure 3.** (A) Synthesis and isolation of  $1[\text{BAR}^{\text{F}}_4]$ . (B)  $^{31}\text{P}\{^1\text{H}\}$  SSNMR (25 °C) of the sieved and graded crystalline polymorphs of  $\alpha\text{-}1[\text{BAR}^{\text{F}}_4]$  and  $\beta\text{-}1[\text{BAR}^{\text{F}}_4]$ .

temperature (−70 °C) solution NMR, ambient temperature solid-state NMR (SSNMR) spectroscopy and single-crystal diffraction. Remarkably, crystalline  $1[\text{BAR}^{\text{F}}_4]$  is also tolerant to degassed  $\text{D}_2\text{O}$  at room temperature as measured by NMR spectroscopy after 1 week (Figures S13–S16). Solution NMR data (−70 °C,  $\text{CD}_2\text{Cl}_2$ ) are in full agreement with the reported literature values.<sup>48</sup> In the  $^1\text{H}$  NMR spectrum the Ir–hydride is observed at  $\delta$  −41.85 and Ir–methyl at  $\delta$  1.85. A single environment is observed in the  $^{31}\text{P}\{^1\text{H}\}$  NMR spectrum at  $\delta$  184.3. In contrast,  $^{31}\text{P}\{^1\text{H}\}$  SSNMR spectroscopy revealed that this initially isolated crystalline material is dimorphic. This is shown by the observation of two distinct sets of tightly coupled AB doublets, centered at  $\delta$  187.5,  $\beta\text{-}1[\text{BAR}^{\text{F}}_4]$ , and  $\delta$  182.9,  $\alpha\text{-}1[\text{BAR}^{\text{F}}_4]$ . Each shows *trans*  $^{31}\text{P}\text{-}^{31}\text{P}$  coupling [ $J(\text{PP}) \sim 340$  Hz], suggesting crystallographically inequivalent phosphine groups for each polymorph. While these polymorphs could not be distinguished visually, they could be reliably separated by graded sieving at ambient temperature (Figure S1). Crystallites of greater than 0.25 mm consist of the major, pure, polymorph,  $\alpha\text{-}1[\text{BAR}^{\text{F}}_4]$ , and could be isolated in  $\sim 90\%$  overall yield on the  $\sim 1$  g scale. Crystallites of less than 0.25 mm are a mixture of  $\alpha$ - and  $\beta$ -forms, Figure 3B. As different morphologies are likely to display different stabilities and reactivity profiles in single-crystal solid/gas reactions,<sup>49,54,79–83</sup> the isolation of a single polymorph,  $\alpha\text{-}1[\text{BAR}^{\text{F}}_4]$ , provides a consistent framework for subsequent reactivity studies.

The previously reported solid-state structure of  $1[\text{BAR}^{\text{F}}_4]$ ,<sup>48</sup> as determined from crystals recrystallized at low temperature from  $\text{CH}_2\text{Cl}_2/\text{diethyl ether}$ , contains a molecule of solvent ( $\text{CH}_2\text{Cl}_2$ ) in the lattice while the Ir–hydride was not located. We have recollected the structure (at −163 °C) using material of the major polymorph that was crystallized at −40 °C using  $1,2\text{-F}_2\text{C}_6\text{H}_4/\text{heptane}$  followed by graded sieving (crystals of greater than 0.25 mm). The structure shows (Figure S91) that single-crystals of phase-pure  $\alpha\text{-}1[\text{BAR}^{\text{F}}_4]$  ( $P2_1/n$  space group) contain no lattice solvent, which removes potential complications in subsequent SC-SC reactivity that are associated with loss of solvent.<sup>82</sup> There is no crystallographically imposed symmetry, consistent with the inequivalent  $^{31}\text{P}$  environments observed in the SSNMR (Figure 3B). However, despite the structural refinement being good [ $R_{\text{int}} = 3.04\%$ ;  $R(2\sigma) = 3.24\%$ ] the hydride ligand could not be located. The position of the hydride above or below the Ir(PONOP)CH<sub>3</sub>-plane is nondegenerate in the solid-state. While there was no indirect evidence for Ir–H disorder from  $^{31}\text{P}\{^1\text{H}\}$  or  $^{13}\text{C}\{^1\text{H}\}$  SSNMR spectroscopy (Figures 3B, S6 and S9) the location of the hydride was thus unresolved.

Precise determination of the position of the hydride ligand came from a single-crystal neutron diffraction study of  $\alpha\text{-}1[\text{BAR}^{\text{F}}_4]$ . Single crystals ( $1.0 \times 1.2 \times 1.8$  mm), that had been stored at ambient temperature under argon, were studied using Laue neutron diffraction at −163 °C, Figure 4A. This revealed the same overall structure as from the single-crystal X-ray experiment, with the hydride and methyl group hydrogens additionally directly located and freely refined with no evidence for disorder [Ir–H1, 1.529(6) Å]. The Ir–C1 distance, 2.096(3) Å, is consistent with an Ir(III)–CH<sub>3</sub> group<sup>45,84</sup> and not Ir(I)⋯H<sub>4</sub>C, which would be expected to have a longer Ir⋯C distance of at least 2.3 Å.<sup>46</sup>

The anions surrounding the cation in  $\alpha\text{-}1[\text{BAR}^{\text{F}}_4]$  form a twisted, pseudo cubic arrangement, Figure 4C, with each cation sitting in an irregular quadrilateral face of  $[\text{BAR}^{\text{F}}_4]^-$  anions. While this pattern is unusual in SMOM, with

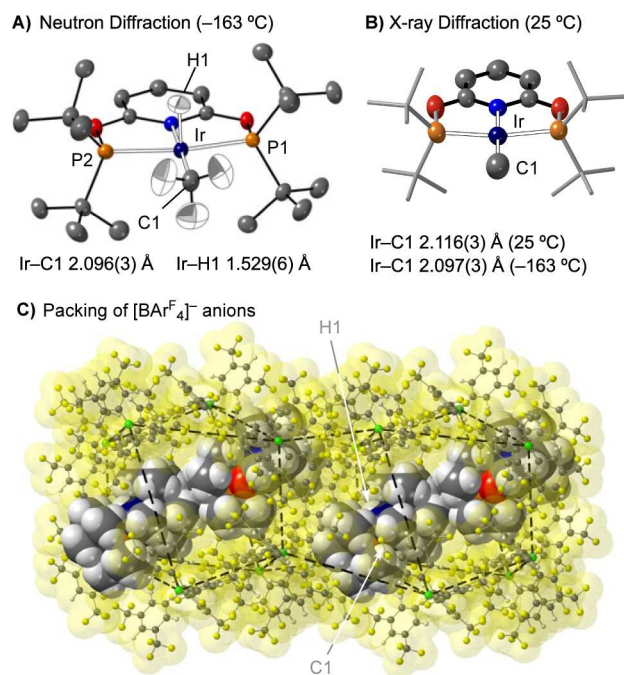


**Figure 4.** Structure of the cation in  $\alpha\text{-1}[\text{BAr}^{\text{F}}_4]$  as determined by single-crystal neutron diffraction at  $-163\text{ }^{\circ}\text{C}$  (A) and X-ray diffraction at  $25\text{ }^{\circ}\text{C}$  (B). Displacement ellipsoids at the 50% probability level, selected H atoms shown. (C) Packing arrangement of  $[\text{BAr}^{\text{F}}_4]^-$  anions in  $\alpha\text{-1}[\text{BAr}^{\text{F}}_4]$ , with H1 and C1 highlighted. Cation atoms and anion molecular surfaces shown at van der Waals radii.

$\sim$ octahedral,<sup>54,56,62</sup> and  $\sim$ bicapped square prismatic,<sup>76,77,82</sup> more common, similar arrangements have been noted previously.<sup>85</sup> While the other polymorph  $\beta\text{-1}[\text{BAr}^{\text{F}}_4]$  (using graded crystallites of less than 0.25 mm) could not be isolated in compositionally pure form separated from  $\alpha\text{-1}[\text{BAr}^{\text{F}}_4]$ , screening of individual single crystals allowed for its structure to be determined (Figures S94 and S95). This showed a bicapped square prismatic arrangement of  $[\text{BAr}^{\text{F}}_4]^-$  anions around two crystallographically equivalent cations,<sup>64,76,77</sup> in the  $C2/c$  space group. The Ir(I)-cation is essentially the same in both polymorphs.

**Variable Temperature X-ray Diffraction and SSNMR, Evidence for a Dynamic Equilibrium That Accesses an Ir(I) $\sigma$ -Methane Complex.** In  $\text{CDCl}_2\text{F}$  solution it has been determined, using quantitative EXSY NMR experiments, that rapid site exchange between Ir-H and Ir-Me occurs at  $-105\text{ }^{\circ}\text{C}$  for  $1[\text{BAr}^{\text{F}}_4]$  with a barrier of 9.3(4) kcal/mol, via an Ir(I)  $\sigma$ -methane intermediate.<sup>48</sup> While this  $\sigma$ -methane complex is  $\sim 5$  kcal/mol higher in energy (gas-phase calculations on a truncated model<sup>46</sup>), we were interested to see if an ambient temperature single-crystal X-ray diffraction experiment revealed that this exchange process also occurred in *crystallo*. Such an exchange would be signaled by a lengthening of the Ir $\cdots$ C distance at higher temperatures, as a larger proportion of the  $\sigma$ -methane complex would be present in any dynamic admixture. Aside from the expected small increase in unit cell volume (4%), the structure collected at  $+25\text{ }^{\circ}\text{C}$  shows a statistically significant ( $3\sigma$ ) but very small change in the Ir-C bond metrics: Ir-C1 = 2.116 (3) Å, Figure 4B. While very small, this nevertheless supports a dynamic reductive coupling to form a  $\sigma$ -methane complex is occurring in the solid-state. However, if such a process is occurring then the equilibrium position at 298 K must still favor the methyl-hydride structural

extreme. As NMR spectroscopy is potentially more sensitive to small changes in the weighted-average equilibrium position of the Ir-CH<sub>3</sub> group,<sup>86</sup> the  $^{13}\text{C}\{^1\text{H}\}$  SSNMR spectrum of  $\alpha\text{-1}[\text{BAr}^{\text{F}}_4]$  was recorded at  $25\text{ }^{\circ}\text{C}$  and  $-80\text{ }^{\circ}\text{C}$ , Figures 5A,B.

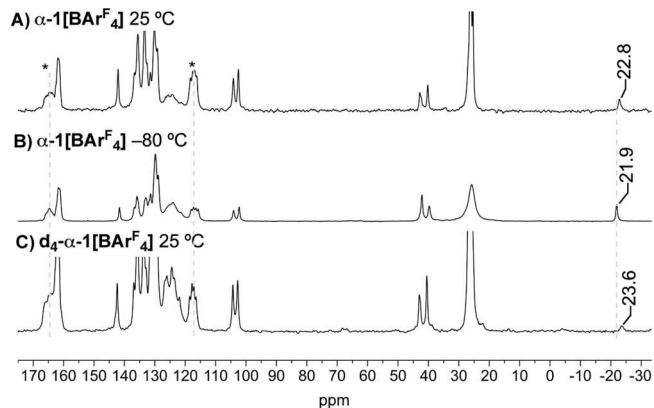


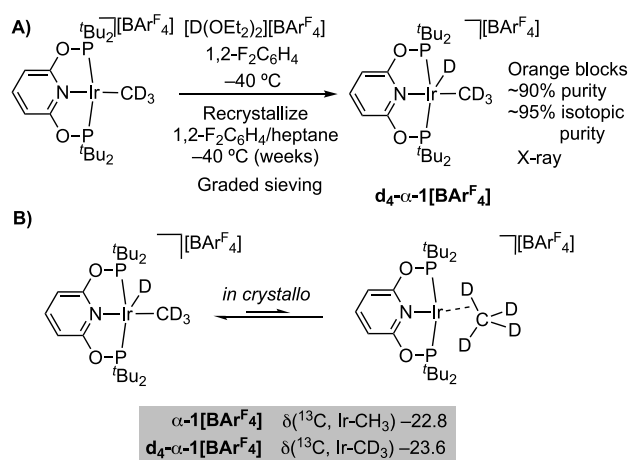
**Figure 5.** Variable temperature  $^{13}\text{C}\{^1\text{H}\}$  CPTOSS (total suppression of side-bands) SSNMR spectra of  $\alpha\text{-1}[\text{BAr}^{\text{F}}_4]$  and  $d_4\text{-}\alpha\text{-1}[\text{BAr}^{\text{F}}_4]$ . \*Selected peaks assigned to  $[\text{BAr}^{\text{F}}_4]^-$ . Dotted lines to guide the eye. Referenced to adamantane (external).

These data demonstrate a small, but significant, upfield chemical shift change of the Ir-CH<sub>3</sub> signal on warming, moving from  $\delta -21.9$  to  $\delta -22.8$ . As an Ir(I)  $\sigma$ -methane complex is expected to have a  $^{13}\text{C}$  chemical shift of  $\sim \delta -40$  to  $-50$ ,<sup>28,29,31</sup> and a cationic Ir(III)-CH<sub>3</sub> would be observed at lower field  $\sim \delta -20$ ,<sup>84</sup> this suggests a small shift in the weighted-average position of a dynamic equilibrium toward the  $\sigma$ -methane complex at room temperature. The signals due to the  $[\text{BAr}^{\text{F}}_4]^-$  anions do not shift significantly.

These observations are consistent with a kinetically accessible  $\sigma$ -methane complex being in rapid equilibrium with a thermodynamically favored ground-state methyl-hydride in the solid-state. As shown next, isotopic labeling studies, reactivity profiles and periodic DFT calculations support this hypothesis.

**Synthesis of  $d_4\text{-}\alpha\text{-1}[\text{BAr}^{\text{F}}_4]$ . Isotopic Perturbation of Equilibrium in the Solid-State.** The  $d_4$ -isotopologue of  $1[\text{BAr}^{\text{F}}_4]$  was prepared by addition of  $[\text{D}(\text{OEt}_2)_2][\text{BAr}^{\text{F}}_4]$ <sup>87</sup> to Ir(<sup>t</sup>Bu-PONOP)(CD<sub>3</sub>)<sup>48</sup> in 1,2- $\text{F}_2\text{C}_6\text{H}_4$  solvent at  $-40\text{ }^{\circ}\text{C}$  (Scheme 1A), and isolated as a crystalline solid from a low-temperature recrystallization, followed by graded sieving (crystals greater than 0.25 mm). Solution NMR data ( $\text{CD}_2\text{Cl}_2$ ,  $-95\text{ }^{\circ}\text{C}$ ) show that  $[\text{Ir}(\text{tBu-PONOP})(\text{CD}_3)\text{D}][\text{BAr}^{\text{F}}_4]$ ,  $d_4\text{-}1[\text{BAr}^{\text{F}}_4]$ , is formed in  $\sim 90\%$  chemical and  $\sim 95\%$  isotopic purity, alongside minor impurities, including cyclo-metalated  $2[\text{BAr}^{\text{F}}_4]$  ( $\sim 2\%$ ).<sup>88</sup>  $^{31}\text{P}\{^1\text{H}\}$  SSNMR spectroscopy of crystalline material (Figures S32) shows that the  $\alpha$ -polymorph is formed,  $d_4\text{-}\alpha\text{-1}[\text{BAr}^{\text{F}}_4]$ .

If a rapid, and reversible equilibrium was occurring between an Ir(III)-methyl-hydride and an Ir(I)  $\sigma$ -methane complex, as, at a first approximation,<sup>89</sup> D prefers to reside in the higher bond-strength oscillator (i.e., C-D rather than Ir-D) an isotopic perturbation of equilibrium may be expected for  $d_4\text{-}\alpha\text{-1}[\text{BAr}^{\text{F}}_4]$ ,<sup>89-91</sup> that would bias toward the  $\sigma$ -methane complex. SSNMR spectroscopy supports such a perturbation, as the room temperature  $^{13}\text{C}\{^1\text{H}\}$  SSNMR spectrum shows the Ir-CD<sub>3</sub> signal shifted to higher field compared with the protio-analog ( $\delta -23.6$  versus  $\delta -22.8$  respectively), Figure 5C and Scheme 1B.

**Scheme 1. (A) Synthesis of  $d_4$ - $\alpha$ -1[ $\text{BAR}^{\text{F}}_4$ ]; (B) Proposed Isotopic Perturbation of Equilibrium at 25 °C**


Chemical shift perturbations, with and without isotopic labeling, have been noted as being diagnostic of the existence of rapid oxidative cleavage/reductive bond formation equilibria occurring in solution, for example in  $(\text{Cp}^{\text{R}})_2\text{Nb}(\text{H}_2\text{B}(\text{O}_2\text{C}_6\text{H}_3\text{R}'))$  ( $\text{Cp}^{\text{R}} = \text{C}_5\text{H}_5, \text{C}_5\text{Me}_5, \text{R}' = \text{H}, \text{tBu}$ ) between Nb(V)-dihydride boryl and Nb(III)-hydrido borate structures.<sup>86,92</sup> Reversible reductive elimination has recently been reported for  $[\text{Ir}(\text{tPr-PNP})(\text{SiR}_3)(\text{CH}_3)][\text{BAR}^{\text{F}}_4]$  pincer complexes, closely related to  $1[\text{BAR}^{\text{F}}_4]$ .<sup>84</sup> While the chemical shift changes observed here are small, that they can be observed at all at room temperature is due to the stabilizing effect of the solid-state crystalline environment, which means that  $1[\text{BAR}^{\text{F}}_4]$  or  $d_4$ - $1[\text{BAR}^{\text{F}}_4]$  do not lose methane readily at room temperature *in crystallo*. However, on relatively mild heating methane is reversibly lost in a SC-SC transformation to form the operationally unsaturated cyclometalated complex,  $2[\text{BAR}^{\text{F}}_4]$ , as described next.

**Methane Reductive Elimination and Cyclometalation *In Crystallo*. Synthesis and Characterization of  $[\text{Ir}(\text{cyclo-}^t\text{Bu-PONOP}')\text{H}][\text{BAR}^{\text{F}}_4]$ .** Heating single crystals of  $\alpha$ -1[ $\text{BAR}^{\text{F}}_4$ ] to 80 °C under a dynamic high vacuum ( $5 \times 10^{-6}$  mbar) for 3 days (200 mg scale) resulted in the formation of Ir(III)-cyclometalated  $[\text{Ir}(\text{cyclo-}^t\text{Bu-PONOP}')\text{H}][\text{BAR}^{\text{F}}_4]$ ,  $2[\text{BAR}^{\text{F}}_4]$ , in 99% recovered yield as single-crystalline pale orange blocks,  $[\text{cyclo-}^t\text{Bu-PONOP}' = \kappa^4\text{-2-}(^t\text{Bu}(\text{H}_2\text{CCMe}_2)\text{-PO})\text{-6-}(^t\text{Bu}_2\text{PO})\text{C}_5\text{H}_3\text{N}]$ .<sup>93</sup> This SC-SC procedure is repeatable (over 10 times) and has been performed on sample sizes of 0.1–0.2 g (1 to 3 days respectively). Figure 6 shows the solid-state structure determined for the cation in  $2[\text{BAR}^{\text{F}}_4]$ .

The single crystal X-ray diffraction analysis of  $2[\text{BAR}^{\text{F}}_4]$  (−163 °C) shows that the  $\alpha$ -crystal form from the starting material is retained (Figure S97), and the unit cell volume is essentially unchanged ( $\Delta V = -0.8\%$ ). Loss of methane has occurred, and one of the  $^t\text{Bu}$  groups has undergone a cyclometalation<sup>94</sup> to form the corresponding Ir(III)–alkyl hydride. The solid-state structure shows a superposition of chemically equivalent isomers, arising from C–H activation of distinct  $^t\text{Bu}$  groups. The best model [ $R_{\text{int}} = 3.1\%$ ;  $R(2\sigma) = 3.84\%$ ] converges to a two site disorder in which  $^t\text{Bu}$  groups from the same phosphine (P1) have undergone C–H activation and cyclometalation in the apical positions of the complex, i.e., above/below the PONOP–Ir plane. The hydride was not located, but is likely situated *trans* to the pyridyl nitrogen, consistent with its rather low field chemical shift and

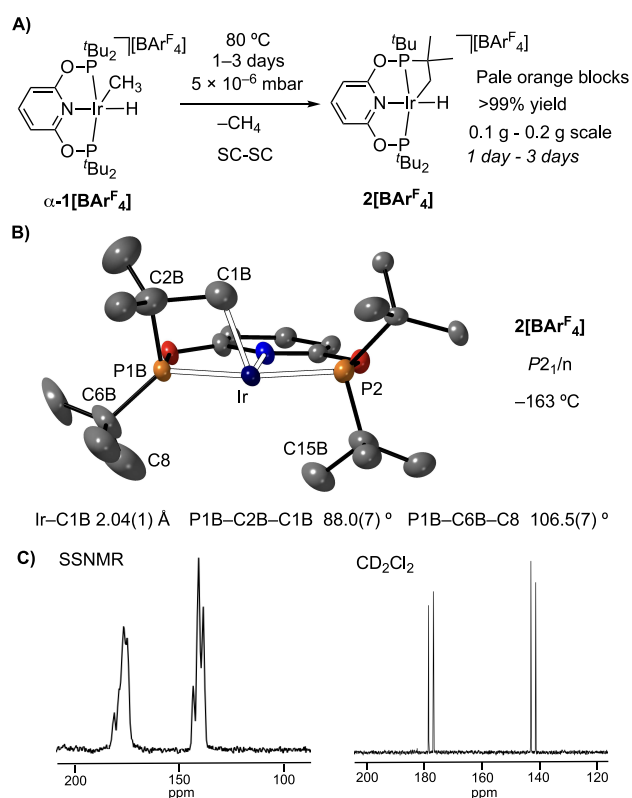


**Figure 6.** (A) Synthesis of  $2[\text{BAR}^{\text{F}}_4]$ . (B) Structure of the cation in one of the disorder components of  $2[\text{BAR}^{\text{F}}_4]$  from single crystal X-ray diffraction. Displacement ellipsoids shown at the 30% probability levels. H-atoms omitted for clarity. (C)  $^{31}\text{P}\{^1\text{H}\}$  SSNMR (left) and solution NMR (right) spectra at 25 °C of  $2[\text{BAR}^{\text{F}}_4]$ .

$J(\text{PH})$  coupling constants (*vide infra*). The Ir–C1B distance [2.039(13) Å] and compressed P1B–C2B–C1B angle [88.0(7)°] are consistent with cyclometalation. There is a relatively close approach of another  $^t\text{Bu}$  methyl group to the vacant site *trans* to C1B [ $\text{Ir}\cdots\text{C15B} = 2.884(16)$  Å] which may suggest an agostic interaction.<sup>95</sup> Although there is no evidence from solution NMR spectroscopy for this, a weak agostic interaction is computed in the static structure (see below). Closely related cyclometalated Ir(III) pincer complexes show similar structures in terms of apical C–H activation, and Ir–C distances.<sup>96–101</sup> While this superposition of disordered components means the detailed structural metrics should be interpreted with caution, the SC-SC reactivity is unambiguous: on heating  $\alpha$ -1[ $\text{BAR}^{\text{F}}_4$ ] to 80 °C under high vacuum methane loss results in conversion to cyclometalated  $2[\text{BAR}^{\text{F}}_4]$ . Further confirmation of the cyclometalated motif came from dissolving crystalline  $2[\text{BAR}^{\text{F}}_4]$  in MeCN and the isolation of, structurally characterized,  $2\text{-MeCN}[\text{BAR}^{\text{F}}_4]$ ,  $[\text{Ir}(\text{cyclo-}^t\text{Bu-PONOP}')\text{H}(\text{NCMe})][\text{BAR}^{\text{F}}_4]$ , Figure S98, as the only product.<sup>102</sup>

Room temperature solid-state and solution NMR spectroscopies show that this conversion to  $2[\text{BAR}^{\text{F}}_4]$  is quantitative, and data are similar to those for other cyclometalated Ir(III) pincer complexes.<sup>96–101</sup> In the  $^{31}\text{P}\{^1\text{H}\}$  SSNMR spectrum multiple overlapping environments are observed, centered at  $\delta$  175 and 140. The solution  $^{31}\text{P}\{^1\text{H}\}$  NMR spectrum is much simpler, with signals observed at  $\delta$  177.7 and 141.8 that show *trans*  $^{31}\text{P}$ – $^{31}\text{P}$  coupling [ $J(\text{PP}) = 345$  Hz], Figure 6C. These data are consistent with the disorder associated with cyclometalation in the solid-state, which is resolved in solution as the different components become degenerate. The cyclo-

metalated methylene is observed at  $\delta -3.7$  (br) in the  $^{13}\text{C}\{^1\text{H}\}$  SSNMR spectrum and  $\delta -2.5$  [dd,  $J(\text{CP}) = 26$ , 2 Hz] in solution. In the  $^1\text{H}$  NMR spectrum the Ir–H hydride is observed as an apparent triplet  $\delta -9.24$  [dd,  $J(\text{HP}) = 11.3$  Hz], and the diastereotopic methylene group at  $\delta 3.09$  and 0.79.

Combined, these data also show that there is no fast exchange between the cyclometalated and other  $^t\text{Bu}$  groups on the NMR time scale at room temperature *in crystallo* or in solution, unlike for some other operationally unsaturated  $^t\text{Bu}$ -cyclometalated complexes that undergo fast exchange in solution.<sup>72,103,104</sup> As such a reversible exchange likely operates via low coordinate, low oxidation state, intermediates, we hypothesized that such an intermediate may be accessible from  $2[\text{BAR}^{\text{F}}_4]$  on heating *in crystallo* – informed by the reactivity of  $1[\text{BAR}^{\text{F}}_4]$ , and the reactivity of related cyclo-metalated complexes in solution.<sup>72,104</sup> This was initially probed by reactivity with  $\text{N}_2$  and CO, coordination of which would trap out such an intermediate.

**In Crystallo Reactivity of  $[\text{Ir}(\text{cyclo-}^t\text{Bu-PONOP})\text{H}][\text{BAR}^{\text{F}}_4]$  with CO,  $\text{N}_2$ .** The reaction of crystalline  $2[\text{BAR}^{\text{F}}_4]$  with  $\text{N}_2$  (80 °C, 7 days, flask open to an  $\text{N}_2$ -filled glovebox) is a SC-SC transformation, that forms  $[\text{Ir}(^t\text{Bu-PONOP})(\kappa^1\text{-N}_2)][\text{BAR}^{\text{F}}_4]$ ,  $3[\text{BAR}^{\text{F}}_4]$ . No reaction occurs at ambient temperature. A single-crystal X-ray diffraction analysis, Figure 7A, shows a  $\kappa^1\text{-N}_2$  ligand [ $\text{N}2\text{--N}3 = 1.120(12)$  Å]; while in

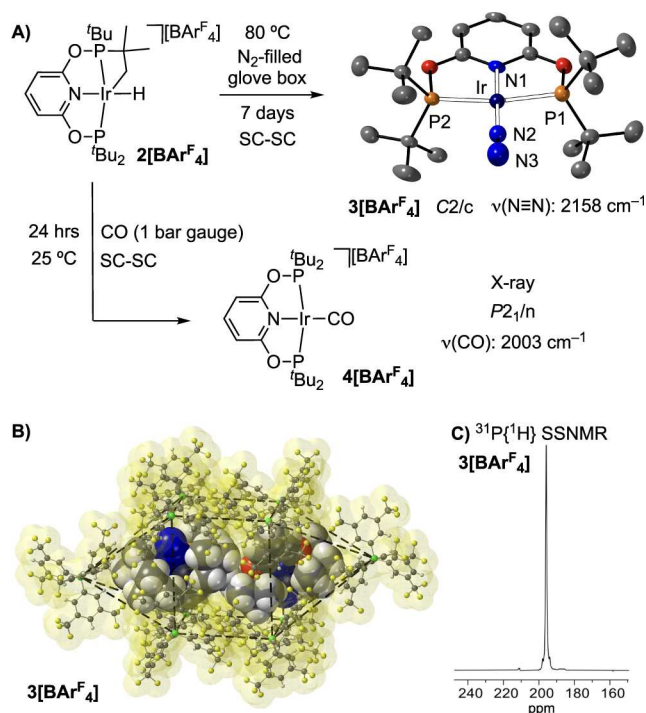


**Figure 7.** (A) SC-SC reactivity of  $2[\text{BAR}^{\text{F}}_4]$  with CO and  $\text{N}_2$ . Solid-state structure of the cation of  $3[\text{BAR}^{\text{F}}_4]$ . Displacement ellipsoids are shown at the 50% level. (B) Packing diagram of  $3[\text{BAR}^{\text{F}}_4]$ . Cation atoms and anion molecular surface shown at van der Waals radii. (C)  $^{31}\text{P}\{^1\text{H}\}$  SSNMR of  $3[\text{BAR}^{\text{F}}_4]$ .

the infrared spectrum the  $\text{N}=\text{N}$  stretch is observed at  $\nu(\text{N}=\text{N})$  2158  $\text{cm}^{-1}$ . The  $\text{N}=\text{N}$  stretch in related pincer complexes  $[\text{Rh}(^t\text{Bu-PONOP})(\kappa^1\text{-N}_2)][\text{BAR}^{\text{F}}_4]$  [ $\nu(\text{N}=\text{N})$  2202  $\text{cm}^{-1}$ ]<sup>75</sup> and  $\text{Ir}(^t\text{Bu-PCP})(\kappa^1\text{-N}_2)$  [ $\nu(\text{N}=\text{N})$  2076  $\text{cm}^{-1}$ ]<sup>105</sup> reflect the back-bonding differences between  $4d/5d$  and cationic/neutral metal centers. Interestingly, there is a space group change on going

from  $2[\text{BAR}^{\text{F}}_4]$  to  $3[\text{BAR}^{\text{F}}_4]$ , from  $P2_1/n$  to  $C2/c$ , the latter the same as  $\beta\text{-1}[\text{BAR}^{\text{F}}_4]$ . This manifests by a change in the anion-packing to a bicapped square prism and a characteristic  $^{31}\text{P}\{^1\text{H}\}$  SSNMR spectrum Figure 7C (cf. Figure 3B). This SC-SC structural adaptivity<sup>80,83</sup> on addition of an external gaseous reagent has been noted before in SMOM systems,<sup>77,106</sup> as is facilitated by the  $-\text{CF}_3$  groups on the  $[\text{BAR}^{\text{F}}_4]^-$  anion that allow for significant plasticity in the single-crystal. There is, however, no significant change in the unit cell volume ( $V/Z = 1496$  Å<sup>3</sup>,  $3[\text{BAR}^{\text{F}}_4]$ ; 1502 Å<sup>3</sup>,  $2[\text{BAR}^{\text{F}}_4]$ ).

This reactivity is consistent with  $2[\text{BAR}^{\text{F}}_4]$  acting as a source of a transient 14-electron Ir(I)  $[\text{Ir}(^t\text{Bu-PONOP})][\text{BAR}^{\text{F}}_4]$ , **III**, by reductive elimination of the cyclometalated group at 80 °C, and that lattice-available  $\text{N}_2$  traps this reactive species by coordination. However, we cannot discount a mechanism in which initial binding of  $\text{N}_2$  to  $2[\text{BAR}^{\text{F}}_4]$  promotes reductive elimination (see Computational Studies Section). In support of this alternative mechanism being plausible, the reaction of CO with  $2[\text{BAR}^{\text{F}}_4]$  does not require heating and occurs over a much shorter time scale (24 h).

Addition of CO (1 bar gauge) to single-crystals of  $2[\text{BAR}^{\text{F}}_4]$  for 24 h at 25 °C (unoptimized) results in the quantitative formation of the known<sup>45</sup> complex  $[\text{Ir}(^t\text{Bu-PONOP})(\text{CO})][\text{BAR}^{\text{F}}_4]$ ,  $4[\text{BAR}^{\text{F}}_4]$ , Figure 7A. This is a SC-SC transformation that retains the same anion-packing and space group ( $P2_1/n$ ) of the starting material, as shown by the solid-state structure (Figures S100 and S102). Solution and SSNMR data confirm that C–H reductive elimination has occurred from  $2[\text{BAR}^{\text{F}}_4]$ . This presumably occurs via coordination of CO to form a six-coordinate Ir(III)-cyclometalated complex,<sup>100</sup> that then undergoes reductive elimination.<sup>107</sup> While it is generally accepted that reductive elimination in  $d^6$  complexes is favored from 5-coordinate species,<sup>108</sup> ligand-assisted reductive elimination from 6-coordinate complexes can occur by addition of ligands such as alkenes or  $\text{H}_2$ .<sup>109,110</sup> Addition of CO has also been shown to promote reductive elimination in a closely related neopentyl cyclometalated Ir-pincer-hydride complex.<sup>99,100</sup>

While CO and  $\text{N}_2$  are similar sizes, studies on microporous MOF systems show that CO may diffuse more slowly than  $\text{N}_2$  through a relatively confined lattice.<sup>111,112</sup> While this suggests that the relative rates of reaction observed here are not diffusion limited,<sup>67</sup> the effects of local concentration and the space-group change associated with  $3[\text{BAR}^{\text{F}}_4]$  cannot be discounted and are currently unresolved.

**In Crystallo Reactivity of  $[\text{Ir}(\text{cyclo-}^t\text{Bu-PONOP})\text{H}][\text{BAR}^{\text{F}}_4]$  with  $\text{CH}_4$ . Reversible Methane Activation in a SC-SC Transformation.** To further test the hypothesis that reductive elimination of the cyclometalated  $^t\text{Bu}$  group can access a transient 14-electron  $[\text{Ir}(^t\text{Bu-PONOP})][\text{BAR}^{\text{F}}_4]$ , **III**, intermediate *in crystallo*, finely crushed  $2[\text{BAR}^{\text{F}}_4]$  ( $\sim 5$  mg) was heated to 80 °C under an atmosphere of methane (2 to 8 bar gauge) for 24 h in heavy walled/high pressure NMR tubes, Figure 8A. It was anticipated that, if formed, **III** would react rapidly with methane present in the lattice to reform  $1[\text{BAR}^{\text{F}}_4]$ . After 24 h the resulting solids were analyzed by low temperature solution NMR spectroscopy ( $\text{CD}_2\text{Cl}_2$ ,  $-90$  °C). This showed that  $1[\text{BAR}^{\text{F}}_4]$  is indeed formed cleanly, and that higher methane pressures result in increasing proportions of  $1[\text{BAR}^{\text{F}}_4]$  compared with  $2[\text{BAR}^{\text{F}}_4]$ : from a ratio of 40:60 at 2 bar gauge, to 68:32 at 8 bar gauge, Figure 8B. A single crystal X-ray diffraction experiment (8 bar gauge  $\text{CH}_4$ , Figure S60) solved as a mixture of  $\alpha\text{-1}[\text{BAR}^{\text{F}}_4]:2[\text{BAR}^{\text{F}}_4]$  with the methyl group (C1) refining for 55% occupancy – in good agreement

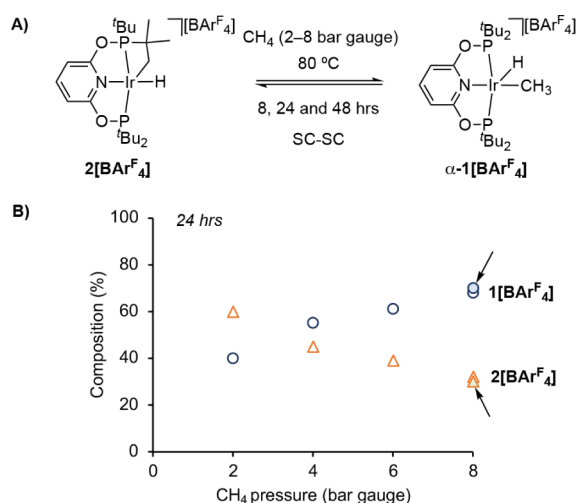


**Figure 8.** (A) Addition of CH<sub>4</sub> to 2[BArF<sub>4</sub>] in the crystalline solid-state. (B) Plot of relative proportions of α-1[BArF<sub>4</sub>] and 2[BArF<sub>4</sub>] as measured by <sup>1</sup>H NMR spectroscopy (−90 °C, CD<sub>2</sub>Cl<sub>2</sub>). Solid markers, highlighted with arrows, indicate the reverse reaction (i.e., starting from α-1[BArF<sub>4</sub>]) under the same conditions of temperature, pressure (8 bar gauge) and time.

with the NMR data. Shorter reaction times (8 h) resulted in reduced conversion to 1[BArF<sub>4</sub>] while longer times (48 h) were no different, showing the data at 24 h represents the equilibrium position. There was no reaction at ambient temperature.

These results suggest a dynamic, pressure-dependent, equilibrium exists between 1[BArF<sub>4</sub>] and 2[BArF<sub>4</sub>]/CH<sub>4</sub> at 80 °C *in crystallo*. This hypothesis is supported by two additional observations. First, addition of 8 bar gauge CH<sub>4</sub> to single crystals of α-1[BArF<sub>4</sub>] (~6 mg) at 80 °C results in essentially the same ratio as observed when starting with 2[BArF<sub>4</sub>] under the same conditions (Figure 8B, solid-markers). Second, addition of CH<sub>4</sub> to 2[BArF<sub>4</sub>] (~20 mg) to form an equilibrium mixture with α-1[BArF<sub>4</sub>], followed by application of high vacuum returns 2[BArF<sub>4</sub>], as shown by <sup>31</sup>P{<sup>1</sup>H} SSNMR spectra of crystalline materials after each step (Figure 9).

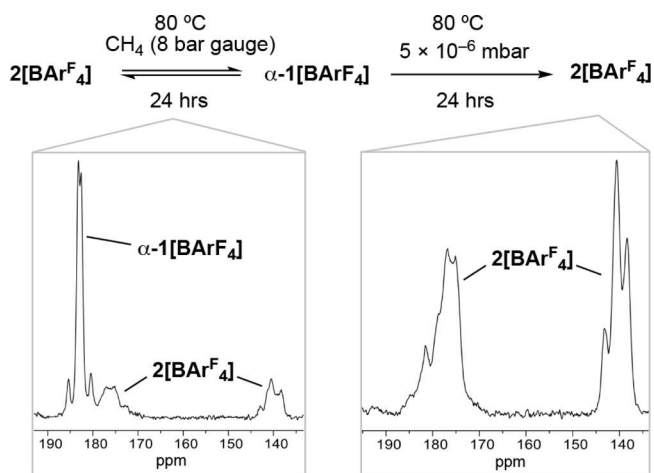


**Figure 9.** Sequential reaction of crystalline 2[BArF<sub>4</sub>] with CH<sub>4</sub> (8 bar gauge) and then application of a high vacuum. Insets show <sup>31</sup>P{<sup>1</sup>H} SSNMR spectra of each reaction.

Reaction between CD<sub>4</sub> (8 bar gauge, 24 h, 80 °C) and 2[BArF<sub>4</sub>] resulted in a ratio of d<sub>4</sub>-1[BArF<sub>4</sub>]:2[BArF<sub>4</sub>] that was relatively enriched in 2[BArF<sub>4</sub>] compared to the reaction with CH<sub>4</sub> (56:44 versus 68:32 respectively) as measured by low temperature solution NMR spectroscopy (−90 °C, CD<sub>2</sub>Cl<sub>2</sub>) of the dissolved solids. While this is consistent with an equilibrium isotope effect operating, with D preferring to be in the C–D (i.e., CD<sub>4</sub>) rather than Ir–D position,<sup>90,113</sup> the presence of N<sub>2</sub> in the, as received, CD<sub>4</sub> resulted in the formation of significant amounts of the dinitrogen adduct [Ir(t-Bu-PONOP)(κ<sup>1</sup>-N<sub>2</sub>)] [BArF<sub>4</sub>] 3[BArF<sub>4</sub>] (~10%), presumably by intercepting III prior to C–H (or C–D) activation.

There was no D incorporation into the t-Bu groups in the product (<sup>2</sup>H NMR spectroscopy, CD<sub>2</sub>Cl<sub>2</sub>) under these conditions. This was best measured by subsequent solid/gas addition of CO to the D-labeled equilibrium mixture to form a mixture of the room temperature stable complexes 4[BArF<sub>4</sub>] (Figure 7) and [Ir(t-Bu-PONOP)(CO)(CD<sub>3</sub>D)] [BArF<sub>4</sub>], the isotopologue of previously reported [Ir(t-Bu-PONOP)(CO)-(CH<sub>3</sub>H)] [BArF<sub>4</sub>].<sup>45</sup> The lack of measurable H/D exchange into the t-Bu groups supports oxidative addition of methane to a 14-electron [Ir(t-Bu-PONOP)] [BArF<sub>4</sub>] intermediate, rather than a σ-CAM (σ-complex assisted metathesis) mechanism, in which H/D scrambling into the t-Bu groups might be expected.<sup>27</sup>

**Computational Studies.** These experimental observations were explored further with periodic DFT calculations. The computed structures of both α-1[BArF<sub>4</sub>] (neutron) and 2[BArF<sub>4</sub>] show good agreement with experiment.<sup>102</sup> For the 2<sup>+</sup> cation the location of the hydride *trans* to pyridine is confirmed and while some discrepancy is seen in the Ir–C1B distance (calc: 2.10 Å; exp: 2.04(1) Å), this likely reflects the disorder noted in the crystal structure. A weak agostic interaction is computed *trans* to the Ir–C15B bond in 2<sup>+</sup> (C1B–H = 1.14 Å; Ir···H = 2.07 Å), but no agostic interaction is seen in 1<sup>+</sup> (shortest Ir···H<sup>t</sup>Bu contact = 2.86 Å).

Reactivity in the solid-state is modeled at one cation in the unit cell of interest, e.g., CH<sub>4</sub> loss from α-1[BArF<sub>4</sub>] forms one 2<sup>+</sup> cation within the α-1[BArF<sub>4</sub>] unit cell (denoted 2<sup>+</sup>@α-1[BArF<sub>4</sub>], see Figure 10).<sup>114</sup> The most accessible pathway proceeds via reductive coupling to a CH<sub>4</sub> σ-complex, Int(1<sup>+</sup>–2<sup>+</sup>)1 at +9.6 kcal/mol followed by CH<sub>4</sub> dissociation to 14e Int(1<sup>+</sup>–2<sup>+</sup>)2 at 20.7 kcal/mol (intermediate and transition state labels omit the unit cell designation for simplicity). Cyclometalation via TS(1<sup>+</sup>–2<sup>+</sup>)2 at 31.0 kcal/mol leads to 2<sup>+</sup>@α-1[BArF<sub>4</sub>] with an overall free energy change, ΔG, of −0.1 kcal/mol. A transition state for cyclometalation occurring directly at Int(1<sup>+</sup>–2<sup>+</sup>)1 in which CH<sub>4</sub> maintains an interaction with the Ir center was higher in energy (+38.6 kcal/mol) and other alternative pathways (via an Ir(V) intermediate, an Ir(III) σ-CH<sub>4</sub> complex or concerted cyclometalation/CH<sub>4</sub> loss) were also ruled out (Figures S107–S109). The naked [Ir(PONOP)]<sup>+</sup> species Int(1<sup>+</sup>–2<sup>+</sup>)2 (equivalent to 14 electron III) is therefore a key intermediate in the reaction from which rate-limiting C–H activation is accessed via TS(1<sup>+</sup>–2<sup>+</sup>)2 with an overall energy span, ΔG<sup>‡</sup>, of 31.0 kcal/mol. TS(1<sup>+</sup>–2<sup>+</sup>)2 is an early transition state with relatively little C–H bond elongation (1.18 Å) and an Ir···H distance of 1.93 Å. More significant changes involve the Ir–P–C(t-Bu) angles, which evolve from 114.8°/120.0° in Int(1<sup>+</sup>–2<sup>+</sup>)2 through 93.9°/128.9° in TS(1<sup>+</sup>–2<sup>+</sup>)2 to 90.1°/137.1° in 2<sup>+</sup>. The calculations also confirm that the 1<sup>+</sup> cation in α-1[BArF<sub>4</sub>] can readily access a σ-CH<sub>4</sub> complex in a rapid and reversible

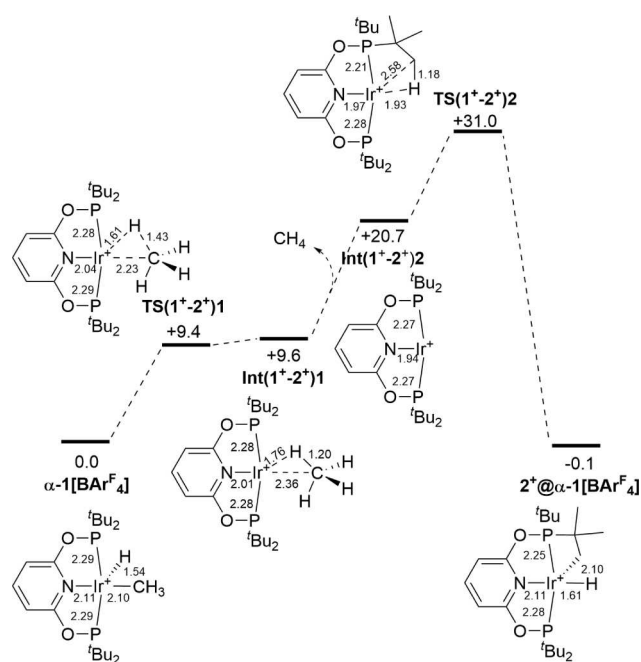


**Figure 10.** Periodic DFT free energy profile (kcal/mol) computed at 80 °C for methane loss from  $\alpha\text{-1}[\text{BARF}_4]$  to give  $2^+\text{@}\alpha\text{-1}[\text{BARF}_4]$ . Structures show key distances (Å) in the reacting cation; intermediate and transition state labels omit the unit cell designation for simplicity. Method: PBE-D3/DZVP-MOLOPT-SR-GTH/GTH-PBE/700 Ry cutoff.

equilibrium that lies toward the Ir hydrido methyl form, as suggested by experiment (Figure 5).

Modeling the reverse reaction, the addition of  $\text{CH}_4$  (1 atm) to one of the cations in  $2[\text{BARF}_4]$  to give  $1^+\text{@}2[\text{BARF}_4]$ , confirms the mechanism in Figure 10: initial C–H coupling forms the equivalent 14-electron  $\text{Int}(2^+-1^+)1$  followed by oxidative addition of  $\text{CH}_4$  (Figure S112). With this model the overall energy span,  $\Delta G^\ddagger$  (relative to  $2[\text{BARF}_4]$ ), is 30.5 kcal/mol and  $\Delta G = +0.8$  kcal/mol. Both models therefore provide barriers commensurate with slow reactivity at 80 °C while the small  $\Delta G$  values reflect the finely balanced equilibria evidenced in Figure 8. Alternative mechanisms, including  $\sigma$ -CAM processes, are again higher in energy; the proposed mechanism is therefore consistent with the exclusive formation of  $[\text{Ir}(\text{tBu-PONOP})(\text{CD}_3)\text{D}][\text{BARF}_4]$  seen experimentally.

Computed profiles for the reactions of  $2[\text{BARF}_4]$  with  $\text{N}_2$  and CO are shown in Figure 11. With  $\text{N}_2$  a 6-coordinate adduct is formed at +5.4 kcal/mol and C–H coupling proceeds through  $\text{TS}(2^+\cdot\text{N}_2\text{-}3^+)$  with an overall barrier of 29.7 kcal/mol. This associative transition state has a somewhat later transition state geometry than  $\text{TS}(1^+-2^+)2$  computed in the unassisted pathway (Figure 10). Both processes have similar overall barriers (within 1 kcal/mol) suggesting the two mechanisms will be competitive. This is consistent with the similar time scales for the reactions of  $2[\text{BARF}_4]$  with  $\text{CH}_4$  and  $\text{N}_2$  observed experimentally. In contrast, CO addition to one of the cations in  $2[\text{BARF}_4]$  is strongly exergonic and first forms  $2^+\cdot\text{CO}$  at  $-32.4$  kcal/mol. The subsequent C–H coupling proceeds with a barrier of only 17.4 kcal/mol and forms  $4^+\text{@}2[\text{BARF}_4]$  at  $-55.5$  kcal/mol. CO therefore plays a significant role in promoting the C–H coupling process. While  $\text{N}_2$  also promotes this step (the barrier for  $2^+\cdot\text{N}_2$  is 24.3 kcal/mol) its effect on the overall energy span is marginal.

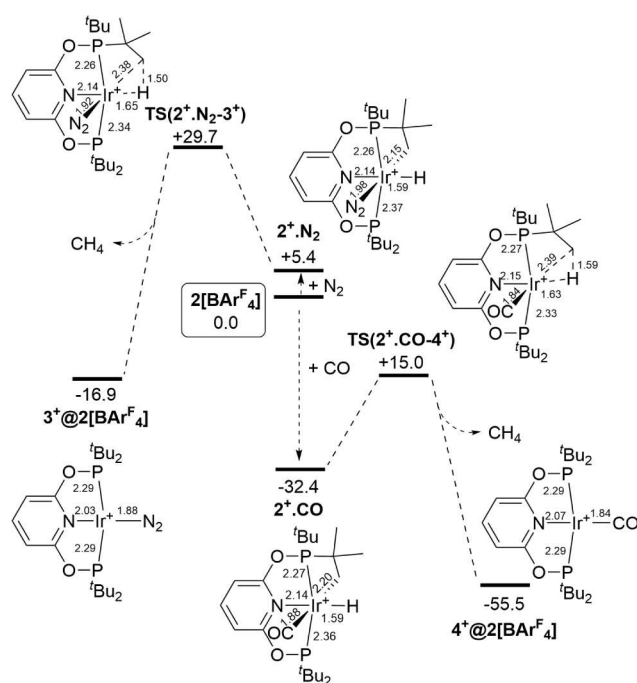


**Figure 11.** Periodic DFT free energy profile (kcal/mol) computed for the reactions of  $2[\text{BARF}_4]$  with  $\text{N}_2$  (1 atm at 80 °C) and CO (1 atm at 25 °C) to form  $3^+\text{@}2[\text{BARF}_4]$  and  $4^+\text{@}2[\text{BARF}_4]$ , respectively. Structures show key distances (Å) in the reacting cation; intermediate and transition state labels omit the unit cell designation for clarity. Method: PBE-D3/DZVP-MOLOPT-SR-GTH/GTH-PBE/700 Ry cutoff.

**Equilibrium Isotope Effects for Reversible Methane Loss in  $[\text{Ir}(\text{tBu-PONOP})\text{MeH}][\text{BARF}_4]$ . Support for Rapid and Reversible Reductive Bond Formation to Form a  $\sigma$ -Methane Complex, Followed by a Slower Dissociative Methane Loss *In Crystallo*.** Experiment and periodic DFT calculations suggest the reversible, and low energy, formation of an intermediate Ir(I)  $\sigma$ -methane complex from  $1[\text{BARF}_4]$ , prior to a higher energy dissociative methane loss to form 14-electron  $[\text{Ir}(\text{tBu-PONOP})][\text{BARF}_4]$ , III. To support this hypothesis experiments were performed using the isotopologue  $\text{d}_4\text{-}\alpha\text{-1}[\text{BARF}_4]$ , Figure 12. First, heating crystalline  $\text{d}_4\text{-}\alpha\text{-1}[\text{BARF}_4]$  under high vacuum at 80 °C for 3 days produces isotopically pure  $2[\text{BARF}_4]$ , with no H/D exchange into the Ir–H unit observed to the detection limit of  $^1\text{H}$  NMR, Figure 12A. This supports reductive elimination of  $\text{CD}_4$  occurring prior to cyclometalation. An alternative  $\sigma$ -CAM mechanism, or an Ir(V) intermediate, would be expected to result in an Ir–D bond being formed.<sup>27</sup> Second, the rapid and reversible formation of an Ir(I)  $\sigma$ -methane complex would be expected to be signaled by an inverse isotope effect being observed for overall methane reductive elimination, i.e., the overall reaction proceeds faster with the deuterated isotopologue.<sup>89–91</sup> This is because subsequent, rate-determining, dissociative loss of methane to form III would be expected to show only a small, if any, isotope dependence, when using  $\text{d}_4\text{-}\alpha\text{-1}[\text{BARF}_4]$ . An equilibrium isotope effect (EIE) arising from preceding reversible reductive bond formation from  $1[\text{BARF}_4]$  would, however, bias the pre-equilibrium toward an Ir(I)  $\sigma$ -methane complex for the deuterated analog, Scheme 2; as discussed for the  $^{13}\text{C}\{^1\text{H}\}$  SSNMR data of  $\alpha\text{-1}[\text{BARF}_4]$  and  $\text{d}_4\text{-}\alpha\text{-1}[\text{BARF}_4]$ . Heating finely crushed samples ( $\sim 14$  mg) of  $\alpha\text{-1}[\text{BARF}_4]$  and  $\text{d}_4\text{-}\alpha\text{-1}[\text{BARF}_4]$  side-by-side at 80 °C under high vacuum for 1

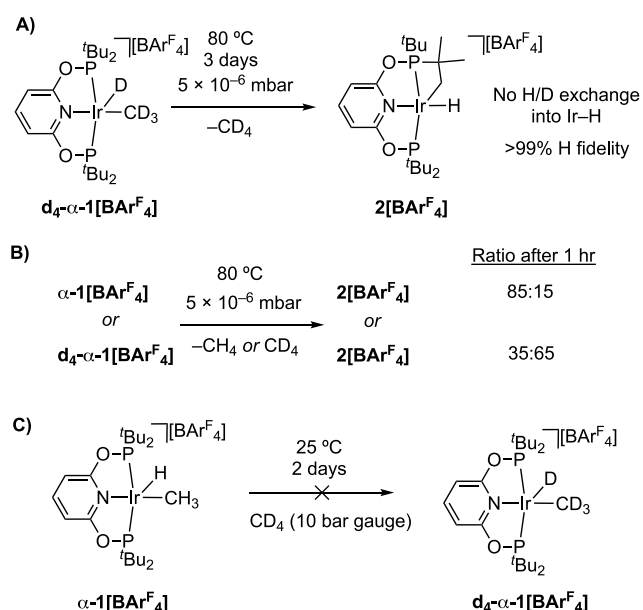
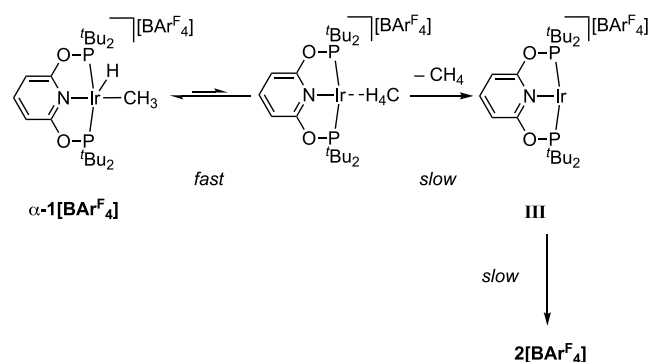


Figure 12. Reactivity of isotopologues of  $\alpha\text{-1}[\text{BAr}^F_4]$ .

**Scheme 2. Pre-Equilibrium before  $\text{CH}_4$  Loss That Results in the Observed EIE (Conditions  $80 \text{ }^\circ\text{C}$ , High Vacuum)**



h, quenching by cooling to ambient temperature and analysis by  $^1\text{H}$  NMR spectroscopy ( $-90 \text{ }^\circ\text{C}$ ,  $\text{CD}_2\text{Cl}_2$ ) showed considerably more methane loss from  $d_4\text{-}\alpha\text{-1}[\text{BAr}^F_4]$  to form  $2[\text{BAr}^F_4]$  compared to  $\alpha\text{-1}[\text{BAr}^F_4]$ , Figure 12B (65% versus 15% respectively). Related inverse isotope effects have previously been measured for the SC-SC hydrogenation, or deuteration, of  $[\text{Rh}(\text{C}_7\text{H}_7\text{PCH}_2\text{CH}_2\text{CH}_2\text{PCy}_2)(\text{cyclooctadiene})][\text{BAr}^F_4]$  to form the corresponding  $\sigma$ -alkane (cyclooctane) complex.<sup>115</sup> Finally, addition of  $\text{CD}_4$  (10 bar gauge) to crystalline  $\alpha\text{-1}[\text{BAr}^F_4]$  at ambient temperature resulted in no exchange to form  $d_4\text{-}\alpha\text{-1}[\text{BAr}^F_4]$  (or any other d-isotopologue), Figure 12C, consistent with a high barrier to dissociative loss of methane from the Ir(I)  $\sigma$ -methane complex.

**Stoichiometric *In Crystallo* Ethane Dehydrogenation with  $[\text{Ir}(\text{cyclo-}^t\text{Bu-PONOP}'\text{H})][\text{BAr}^F_4]$ .** The *in crystallo* reaction between  $2[\text{BAr}^F_4]$  and  $\text{CH}_4$  to form the methyl hydride  $\alpha\text{-1}[\text{BAr}^F_4]$  has been shown to be a finely balanced equilibrium, operating via a 14-electron intermediate, III. Interested in exploring alkane C–H activation with another simple substrate, the reaction of ethane with crystalline  $2[\text{BAr}^F_4]$  was studied, under similar conditions to those used for methane activation. Heating  $2[\text{BAr}^F_4]$  for 3 weeks under 1 bar gauge of ethane did not, however, result in the isolation of the corresponding ethyl hydride complex. Instead the

known<sup>116</sup> ethene and dihydride complexes,  $[\text{Ir}(^t\text{Bu-PONOP})-(\eta^2\text{-H}_2\text{C}=\text{CH}_2)][\text{BAr}^F_4]$   $5[\text{BAr}^F_4]$  and  $[\text{Ir}(^t\text{Bu-PONOP})\text{H}_2][\text{BAr}^F_4]$   $6[\text{BAr}^F_4]$  are formed, Figure 13A.

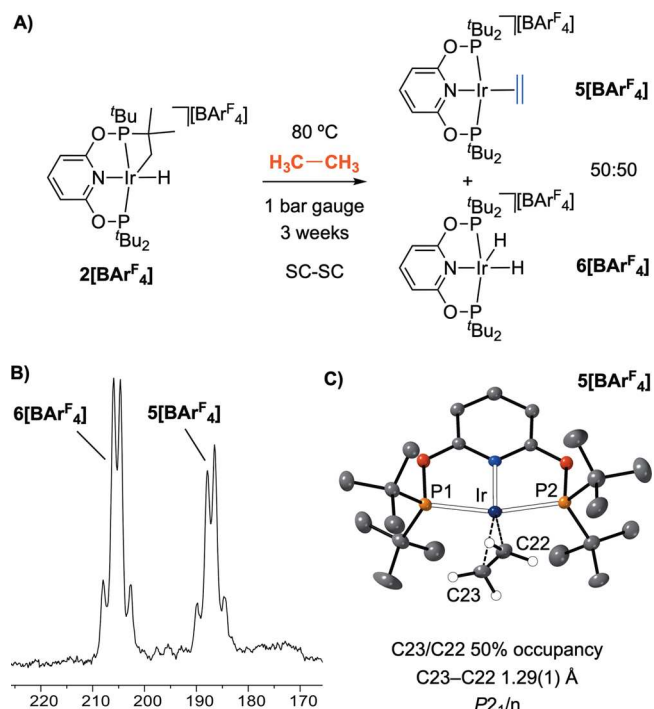
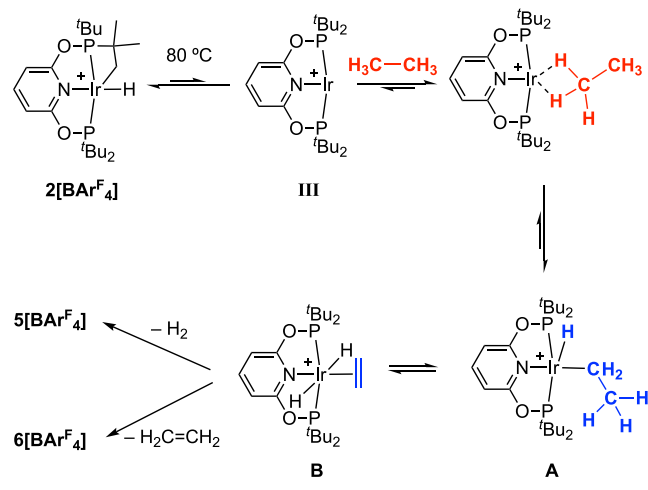


Figure 13. (A) Reaction of  $2[\text{BAr}^F_4]$  with ethane to form  $5[\text{BAr}^F_4]$  and  $6[\text{BAr}^F_4]$ . (B)  $^{31}\text{P}\{^1\text{H}\}$  SSNMR of the crystalline materials post reaction. (C) Solid-state structure of the cations of the admixture of  $5[\text{BAr}^F_4]$  and  $6[\text{BAr}^F_4]$ , with the ethene ligand refined at 50% occupancy.

Solution NMR data for this mixture are the same as previously reported for the individual components,<sup>116</sup> and show  $5[\text{BAr}^F_4]$  and  $6[\text{BAr}^F_4]$  are formed in a  $\sim 50:50$  ratio. In the  $^{31}\text{P}\{^1\text{H}\}$  SSNMR NMR spectrum the two complexes are observed in approximately equal amounts, each as a tightly coupled AB doublet, characteristic of the  $\alpha$ -crystal form, Figure 13B. A single-crystal X-ray diffraction study shows that this transformation is SC-SC, solving as a 50:50 superposition of the two cations in the characteristic  $P2_1/n$  arrangement of  $[\text{BAr}^F_4]^-$  anions, Figure 13C. The ethene ligand in  $5[\text{BAr}^F_4]$  refines at 50% occupancy, while the hydride ligands in  $6[\text{BAr}^F_4]$  were not located.

The proposed mechanism of formation of this mixture is shown in Scheme 3. Reductive elimination in the cyclo-metalated ligand at  $80 \text{ }^\circ\text{C}$  reversibly forms the high energy intermediate III that reacts with lattice-available ethane through C–H activation to initially form an Ir(III) ethyl hydride, A.  $\beta$ -hydrogen transfer then forms a dihydride ethene complex, B. If the barriers to loss of ethene or  $\text{H}_2$  (via an isomerization in B to place the hydrides *cis* to one another) were competitive in the single crystal this would lead to the admixture of  $5[\text{BAr}^F_4]$  and  $6[\text{BAr}^F_4]$ . *In crystallo*  $\text{H}_2$  loss from a complex closely related to B,  $[\text{Ir}(^t\text{Pr-PONOP})(\eta^2\text{-H}_2\text{C}=\text{CHMe})\text{H}_2][\text{BAr}^F_4]$ , has recently been reported, alongside competitive loss of  $\text{H}_2$  or alkene in solution.<sup>76</sup> Further support for this mechanism is provided by the *in situ* observation of the ethyl hydride complex  $[\text{Ir}(^t\text{Bu-PONOP})(\text{H})(\text{CH}_2\text{CH}_3)]\text{-}[\text{NTf}_2]$  (i.e., the cation in A) in solution at very low

### Scheme 3. Proposed Mechanism for the Dehydrogenation of Ethane *In Crystallo*; [BAR<sup>F</sup><sub>4</sub>]<sup>−</sup> Anions Are Not Shown



temperature ( $-100\text{ }^\circ\text{C}$ ) using NMR spectroscopy,<sup>46</sup> which undergoes rapid site exchange between bound C–atoms. DFT calculations suggest this occurs via a  $\beta$ -hydrogen transfer process operating via **B**.

The reaction of  $2[\text{BAR}^{\text{F}}_4]$  with ethane thus represents an *in crystallo* stoichiometric alkane dehydrogenation to form ethene and  $\text{H}_2$ , both of which are trapped in the resulting crystalline products,  $5[\text{BAR}^{\text{F}}_4]$  and  $6[\text{BAR}^{\text{F}}_4]$  respectively. This result adds further support for the formation of a transient 14-electron intermediate, **III**, from reductive elimination from operationally unsaturated  $2[\text{BAR}^{\text{F}}_4]$ , that is irreversibly trapped by reaction with ethane. The slower reaction with ethane compared with methane (3 weeks versus 24 h) is likely a consequence of decreased lattice mobility of the larger ethane, similar to the selectivity observed for the *in crystallo* hydrogenation of ethene over propene using  $\text{Ir}(\text{tBu}-\text{POCOP})-(\kappa^1-\text{N}_2)$ .<sup>78</sup>

## CONCLUSIONS

The coordination and C–H activation of alkanes at transition metal centers relies on the generation of reactive, operationally unsaturated, intermediates in solution. However, such intermediates are in competition with solvent binding, the vast excess of which means that coordination and activation of simple alkanes is challenging. By working *in crystallo*, solvent is removed from the equation, and impediments to alkane binding, C–H activation or overall decomposition are thus attenuated. By generating the operationally unsaturated complexes,  $1[\text{BAR}^{\text{F}}_4]$  and cyclometalated  $2[\text{BAR}^{\text{F}}_4]$ , that function with the retention of crystallinity, methane and ethane activation at a 14-electron Ir(I) center occurs under relatively mild conditions. Such reactivity demonstrates the advantages that synthesis and reactivity in the molecular solid-state provides, especially for the generation of highly reactive intermediates. Extending this to suitable single-crystalline systems that can catalytically activate alkanes is a clear next challenge.

## ASSOCIATED CONTENT

### Supporting Information

The Supporting Information is available free of charge at <https://pubs.acs.org/doi/10.1021/jacs.4c18122>.

NMR spectra, experimental and characterization data for the compounds reported including single-crystal X-ray diffraction studies, and coordinates and energies of computed stationary points (PDF)

Computed geometries (.xyz) as a combined file (ZIP)

## Accession Codes

Deposition Numbers 2410457–2410462 and 2410465 contain the supplementary crystallographic data for this paper. These data can be obtained free of charge via the joint Cambridge Crystallographic Data Centre (CCDC) and Fachinformationszentrum Karlsruhe [Access Structures service](#).

## AUTHOR INFORMATION

### Corresponding Authors

Stuart A. Macgregor – *EaStCHEM School of Chemistry, University of St Andrews, St Andrews KY16 9ST, U.K.*; [orcid.org/0000-0003-3454-6776](https://orcid.org/0000-0003-3454-6776); Email: [sam38@st-andrews.ac.uk](mailto:sam38@st-andrews.ac.uk)

Andrew S. Weller – *Department of Chemistry, University of York, York YO10 5DD, U.K.*; [orcid.org/0000-0003-1646-8081](https://orcid.org/0000-0003-1646-8081); Email: [andrew.weller@york.ac.uk](mailto:andrew.weller@york.ac.uk)

### Authors

Matthew R. Gyton – *Department of Chemistry, University of York, York YO10 5DD, U.K.*; Present Address: School of Chemistry and Molecular Biosciences, Northfields Ave Wollongong, NSW 2522, Australia; [orcid.org/0000-0002-7565-5154](https://orcid.org/0000-0002-7565-5154)

M. Arif Sajjad – *EaStCHEM School of Chemistry, University of St Andrews, St Andrews KY16 9ST, U.K.*; [orcid.org/0000-0002-4119-9912](https://orcid.org/0000-0002-4119-9912)

Daniel J. Storm – *EaStCHEM School of Chemistry, University of St Andrews, St Andrews KY16 9ST, U.K.*; [orcid.org/0009-0009-7189-0008](https://orcid.org/0009-0009-7189-0008)

Kristof M. Altus – *Department of Chemistry, University of York, York YO10 5DD, U.K.*; [orcid.org/0000-0002-8072-8346](https://orcid.org/0000-0002-8072-8346)

Joe C. Goodall – *Department of Chemistry, University of York, York YO10 5DD, U.K.*; [orcid.org/0000-0002-7582-8713](https://orcid.org/0000-0002-7582-8713)

Chloe L. Johnson – *Department of Chemistry, University of York, York YO10 5DD, U.K.*; [orcid.org/0000-0002-0183-2955](https://orcid.org/0000-0002-0183-2955)

Samuel J. Page – *Department of Chemistry, University of Durham, Durham DH1 3LE, U.K.*

Alison J. Edwards – *Australian Centre for Neutron Scattering, Australian Nuclear Science and Technology Organisation, Lucas Heights, New South Wales 2234, Australia*; [orcid.org/0000-0002-5877-0273](https://orcid.org/0000-0002-5877-0273)

Ross O. Piltz – *Australian Centre for Neutron Scattering, Australian Nuclear Science and Technology Organisation, Lucas Heights, New South Wales 2234, Australia*; [orcid.org/0000-0003-0867-3712](https://orcid.org/0000-0003-0867-3712)

Simon B. Duckett – *Department of Chemistry, University of York, York YO10 5DD, U.K.*; [orcid.org/0000-0002-9788-6615](https://orcid.org/0000-0002-9788-6615)

Complete contact information is available at: <https://pubs.acs.org/doi/10.1021/jacs.4c18122>

## Author Contributions

The manuscript was written through contributions of all authors. All authors have given approval to the final version of the manuscript.

## Funding

The EPSRC (EP/W015552/1; EP/W015498/2, DTP to J.C.G.). The Leverhulme Trust (RPG-2020-184). The University of St. Andrews (PhD Scholarship to D.J.S). The Australian Nuclear Science and Technology Organization (ANSTO) is thanked for the generous allocation of beamtime to proposal P16248. This work used the ARCHER2 UK National Supercomputing Service (<https://www.archer2.ac.uk>).<sup>117</sup>

## Notes

The authors declare no competing financial interest.

## ACKNOWLEDGMENTS

The Wild Overseas Scholar's Fund (University of York) is thanked for a generous bursary for J.C.G. to visit ANSTO (Australia) to run neutron diffraction experiments.

## REFERENCES

- (1) Gunsalus, N. J.; Koppaka, A.; Park, S. H.; Bischof, S. M.; Hashiguchi, B. G.; Periana, R. A. Homogeneous Functionalization of Methane. *Chem. Rev.* **2017**, *117*, 8521–8573.
- (2) Cavaliere, V. N.; Mendiola, D. J. Methane: A new frontier in organometallic chemistry. *Chem. Sci.* **2012**, *3*, 3356–3365.
- (3) Labinger, J. A.; Bercaw, J. E. Understanding and exploiting C–H bond activation. *Nature* **2002**, *417*, 507–514.
- (4) Caballero, A.; Pérez, P. J. Methane as raw material in synthetic chemistry: The final frontier. *Chem. Soc. Rev.* **2013**, *42*, 8809–8820.
- (5) Bergman, R. G. C–H activation. *Nature* **2007**, *446*, 391–393.
- (6) Hall, C.; Perutz, R. N. Transition Metal Alkane Complexes. *Chem. Rev.* **1996**, *96*, 3125–3146.
- (7) Cowan, A. J.; George, M. W. Formation and reactivity of organometallic alkane complexes. *Coord. Chem. Rev.* **2008**, *252*, 2504–2511.
- (8) Shteinman, A. A. Shilov alkane platinum chemistry: 45 years. *J. Organomet. Chem.* **2015**, *793*, 34–40.
- (9) Zichittella, G.; Pérez-Ramírez, J. Status and prospects of the decentralised valorisation of natural gas into energy and energy carriers. *Chem. Soc. Rev.* **2021**, *50*, 2984–3012.
- (10) Tang, Y.; Li, Y.; Tao, F. Activation and catalytic transformation of methane under mild conditions. *Chem. Soc. Rev.* **2022**, *51*, 376–423.
- (11) Horn, R.; Schlögl, R. Methane Activation by Heterogeneous Catalysis. *Catal. Lett.* **2015**, *145*, 23–39.
- (12) Wang, B.; Albarracín-Suazo, S.; Pagán-Torres, Y.; Nikolla, E. Advances in methane conversion processes. *Catal. Today* **2017**, *285*, 147–158.
- (13) Ruscic, B. Active Thermochemical Tables: Sequential Bond Dissociation Enthalpies of Methane, Ethane, and Methanol and the Related Thermochemistry. *J. Phys. Chem. A* **2015**, *119*, 7810–7837.
- (14) Smith, K. T.; Berritt, S.; González-Moreiras, M.; Ahn, S.; Smith, M. R.; Baik, M.-H.; Mendiola, D. J. Catalytic borylation of methane. *Science* **2016**, *351*, 1424–1427.
- (15) Fujisaki, H.; Kojima, T. Functionalization of methane using molecular metal complexes as catalysts. *Catal. Sci. Technol.* **2023**, *13*, 4270–4284.
- (16) Staples, O.; Ferrandon, M. S.; Laurent, G. P.; Kanbur, U.; Kropf, A. J.; Gau, M. R.; Carroll, P. J.; McCullough, K.; Sorsche, D.; Perras, F. A. Silica Supported Organometallic Ir<sup>I</sup> Complexes Enable Efficient Catalytic Methane Borylation. *J. Am. Chem. Soc.* **2023**, *145*, 7992–8000.
- (17) Periana, R. A.; Taube, D. J.; Gamble, S.; Taube, H.; Satoh, T.; Fujii, H. Platinum Catalysts for the High-Yield Oxidation of Methane to a Methanol Derivative. *Science* **1998**, *280*, 560–564.
- (18) Cook, A. K.; Schimler, S. D.; Matzger, A. J.; Sanford, M. S. Catalyst-controlled selectivity in the C–H borylation of methane and ethane. *Science* **2016**, *351*, 1421–1424.
- (19) Meyer, D.; Taige, M. A.; Zeller, A.; Hohlfeld, K.; Ahrens, S.; Strassner, T. Palladium Complexes with Pyrimidine-Functionalized N-Heterocyclic Carbene Ligands: Synthesis, Structure and Catalytic Activity. *Organometallics* **2009**, *28*, 2142–2149.
- (20) Caballero, A.; Despagnet-Ayoub, E.; Mar Díaz-Requejo, M.; Díaz-Rodríguez, A.; González-Núñez, M. E.; Mello, R.; Muñoz, B. K.; Ojo, W.-S.; Asensio, G.; Etienne, M. Silver-Catalyzed C–C Bond Formation Between Methane and Ethyl Diazoacetate in Supercritical CO<sub>2</sub>. *Science* **2011**, *332*, 835–838.
- (21) Sadow, A. D.; Tilley, T. D. Homogeneous Catalysis with Methane. A Strategy for the Hydromethylation of Olefins Based on the Nondegenerate Exchange of Alkyl Groups and  $\sigma$ -Bond Metathesis at Scandium. *J. Am. Chem. Soc.* **2003**, *125*, 7971–7977.
- (22) Fujisaki, H.; Ishizuka, T.; Kotani, H.; Shiota, Y.; Yoshizawa, K.; Kojima, T. Selective methane oxidation by molecular iron catalysts in aqueous medium. *Nature* **2023**, *616*, 476–481.
- (23) Waterman, R.  $\sigma$ -Bond Metathesis: A 30-Year Retrospective. *Organometallics* **2013**, *32*, 7249–7263.
- (24) Weller, A. S.; Chadwick, F. M.; McKay, A. I. Transition Metal Alkane-Sigma Complexes: Synthesis, Characterization, and Reactivity. *Adv. Organomet. Chem.* **2016**, *66*, 223–276.
- (25) Kubas, G. J. *Metal Dihydrogen and  $\sigma$ -Bond Complexes*; Kluwer: New York, 2001.
- (26) Hartwig, J. F. Evolution of C–H Bond Functionalization from Methane to Methodology. *J. Am. Chem. Soc.* **2016**, *138*, 2–24.
- (27) Perutz, R. N.; Sabo-Etienne, S.; Weller, A. S. Metathesis by Partner Interchange in  $\sigma$ -Bond Ligands: Expanding Applications of the  $\sigma$ -CAM Mechanism. *Angew. Chem. Int. Ed.* **2022**, *61*, No. e202111462.
- (28) Semprodt, P. J.; Trinh, B. B.; Lovitt, C. F.; Capra, N. E.; Girolami, G. S. An Osmium(II) methane complex: Elucidation of the methane coordination mode. *Sci. Adv.* **2023**, *9*, No. eadg8130.
- (29) Bernskoetter, W. H.; Schauer, C. K.; Goldberg, K. I.; Brookhart, M. Characterization of a Rhodium(I)  $\sigma$ -Methane Complex in Solution. *Science* **2009**, *326*, 553–556.
- (30) Watson, J. D.; Field, L. D.; Ball, G. E. Binding methane to a metal centre. *Nat. Chem.* **2022**, *14*, 801–804.
- (31) Watson, J. D.; Field, L. D.; Ball, G. E. [Fp(CH<sub>4</sub>)]<sup>+</sup>, [ $\eta^5$ -CpRu(CO)<sub>2</sub>(CH<sub>4</sub>)]<sup>+</sup>, and [ $\eta^5$ -CpOs(CO)<sub>2</sub>(CH<sub>4</sub>)]<sup>+</sup>: A Complete Set of Group 8 Metal–Methane Complexes. *J. Am. Chem. Soc.* **2022**, *144*, 17622–17629.
- (32) Cowan, A. J.; Portius, P.; Kawanami, H. K.; Jina, O. S.; Grills, D. C.; Sun, X.-Z.; McMaster, J.; George, M. W. Time-resolved infrared (TRIR) study on the formation and reactivity of organometallic methane and ethane complexes in room temperature solution. *Proc. Nat. Acad. Sci.* **2007**, *104*, 6933–6938.
- (33) Watson, P. L.; Parshall, G. W. Organolanthanides in catalysis. *Acc. Chem. Res.* **1985**, *18*, 51–56.
- (34) Hoyano, J. K.; McMaster, A. D.; Graham, W. A. G. Activation of methane by iridium complexes. *J. Am. Chem. Soc.* **1983**, *105*, 7190–7191.
- (35) Harper, T. G. P.; Shinomoto, R. S.; Deming, M. A.; Flood, T. C. Activation of methane by the reactive intermediate tris(trimethylphosphine)osmium(0). *J. Am. Chem. Soc.* **1988**, *110*, 7915–7916.
- (36) Holtcamp, M. W.; Labinger, J. A.; Bercaw, J. E. C–H Activation at Cationic Platinum(II) Centers. *J. Am. Chem. Soc.* **1997**, *119*, 848–849.
- (37) Cui, W.; Wayland, B. B. Activation of C–H/H–H Bonds by Rhodium(II) Porphyrin Bimetallo-radicals. *J. Am. Chem. Soc.* **2004**, *126*, 8266–8274.

- (38) Jones, W. D.; Maguire, J. A. The activation of methane by rhenium. Catalytic hydrogen/deuterium exchange in alkanes with  $\text{CpRe}(\text{PPh}_3)_2\text{H}_2$ . *Organometallics* **1986**, *5*, 590–591.
- (39) Tsang, J. Y. K.; Buschhaus, M. S. A.; Graham, P. M.; Semiao, C. J.; Semproni, S. P.; Kim, S. J.; Legzdins, P. Facile and Selective Aliphatic C–H Bond Activation at Ambient Temperatures Initiated by  $\text{Cp}^*\text{W}(\text{NO})(\text{CH}_2\text{CMe}_3)(\eta^3\text{-CH}_2\text{CHCHMe})$ . *J. Am. Chem. Soc.* **2008**, *130*, 3652–3663.
- (40) Flores, J. A.; Cavaliere, V. N.; Buck, D.; Pintér, B.; Chen, G.; Crestani, M. G.; Baik, M.-H.; Mindiola, D. J. Methane activation and exchange by titanium-carbon multiple bonds. *Chem. Sci.* **2011**, *2*, 1457–1462.
- (41) Arndtsen, B. A.; Bergman, R. G. Unusually Mild and Selective Hydrocarbon C–H Bond Activation with Positively Charged Iridium(III) Complexes. *Science* **1995**, *270*, 1970–1973.
- (42) Hulvey, Z.; Vlaisavljevich, B.; Mason, J. A.; Tsivion, E.; Dougherty, T. P.; Bloch, E. D.; Head-Gordon, M.; Smit, B.; Long, J. R.; Brown, C. M. Critical Factors Driving the High Volumetric Uptake of Methane in  $\text{Cu}_3(\text{btc})_2$ . *J. Am. Chem. Soc.* **2015**, *137*, 10816–10825.
- (43) Yan, Y.; Kolokolov, D. I.; da Silva, I.; Stepanov, A. G.; Blake, A. J.; Dailly, A.; Manuel, P.; Tang, C. C.; Yang, S.; Schröder, M. Porous Metal–Organic Polyhedral Frameworks with Optimal Molecular Dynamics and Pore Geometry for Methane Storage. *J. Am. Chem. Soc.* **2017**, *139*, 13349–13360.
- (44) Gross, C. L.; Girolami, G. S. M. Alkane Complexes. Rapid Exchange of Hydrogen Atoms between Hydride and Methyl Ligands in  $[(\text{C}_5\text{Me}_5)\text{Os}(\text{dmpm})(\text{CH}_3)\text{H}^+]$ . *J. Am. Chem. Soc.* **1998**, *120*, 6605–6606.
- (45) Campos, J.; Kundu, S.; Pahls, D. R.; Brookhart, M.; Carmona, E.; Cundari, T. R. Mechanism of Hydrogenolysis of an Iridium–Methyl Bond: Evidence for a Methane Complex Intermediate. *J. Am. Chem. Soc.* **2013**, *135*, 1217–1220.
- (46) Walter, M. D.; White, P. S.; Schauer, C. K.; Brookhart, M. Stability and Dynamic Processes in 16VE Iridium(III) Ethyl Hydride and Rhodium(I)  $\sigma$ -Ethane Complexes: Experimental and Computational Studies. *J. Am. Chem. Soc.* **2013**, *135*, 15933–15947.
- (47) Lovitt, C. F.; Capra, N. E.; Lastowski, R. J.; Girolami, G. S. Steric and Electronic Analyses of Ligand Effects on the Stability of  $\sigma$ -Methane Coordination Complexes: A DFT Study. *Organometallics* **2022**, *41*, 3834–3844.
- (48) Bernskoetter, W. H.; Hanson, S. K.; Buzak, S. K.; Davis, Z.; White, P. S.; Swartz, R.; Goldberg, K. I.; Brookhart, M. Investigations of Iridium-Mediated Reversible C–H Bond Cleavage: Characterization of a 16-Electron Iridium(III) Methyl Hydride Complex. *J. Am. Chem. Soc.* **2009**, *131*, 8603–8613.
- (49) Halasz, I. Single-Crystal-to-Single-Crystal Reactivity: Gray, Rather than Black or White. *Cryst. Growth Des.* **2010**, *10*, 2817–2823.
- (50) Young, R. J.; Huxley, M. T.; Pardo, E.; Champness, N. R.; Sumbly, C. J.; Doonan, C. J. Isolating reactive metal-based species in Metal–Organic Frameworks – viable strategies and opportunities. *Chem. Sci.* **2020**, *11*, 4031–4050.
- (51) Fernandez-Bartolome, E.; Martínez-Martínez, A.; Resines-Urien, E.; Piñeiro-Lopez, L.; Costa, J. S. Reversible single-crystal-to-single-crystal transformations in coordination compounds induced by external stimuli. *Coord. Chem. Rev.* **2022**, *452*, 214281.
- (52) Reid, K. A.; Powers, D. C. In crystallo organometallic chemistry. *Chem. Commun.* **2021**, *57*, 4993–5003.
- (53) Pike, S. D.; Thompson, A. L.; Algarra, A. G.; Apperley, D. C.; Macgregor, S. A.; Weller, A. S. Synthesis and Characterization of a Rhodium(I)  $\sigma$ -Alkane Complex in the Solid State. *Science* **2012**, *337*, 1648–1651.
- (54) Chadwick, F. M.; McKay, A. I.; Martínez-Martínez, A. J.; Rees, N. H.; Krämer, T.; Macgregor, S. A.; Weller, A. S. Solid-state molecular organometallic chemistry. Single-crystal to single-crystal reactivity and catalysis with light hydrocarbon substrates. *Chem. Sci.* **2017**, *8*, 6014–6029.
- (55) Docherty, S. R.; Rochlitz, L.; Payard, P.-A.; Copéret, C. Heterogeneous alkane dehydrogenation catalyzed via a surface organometallic chemistry approach. *Chem. Soc. Rev.* **2021**, *50*, 5806–5822.
- (56) Pike, S. D.; Chadwick, F. M.; Rees, N. H.; Scott, M. P.; Weller, A. S.; Krämer, T.; Macgregor, S. A. Solid-State Synthesis and Characterization of  $\sigma$ -Alkane Complexes,  $[\text{Rh}(\text{L}_2)(\eta^2, \eta^2\text{-C}_7\text{H}_{12})][\text{BAR}^{\text{F}}_4]$  ( $\text{L}_2$  = Bidentate Chelating Phosphine). *J. Am. Chem. Soc.* **2015**, *137*, 820–833.
- (57) Sajjad, M. A.; Macgregor, S. A.; Weller, A. S. A comparison of non-covalent interactions in the crystal structures of two  $\sigma$ -alkane complexes of Rh exhibiting contrasting stabilities in the solid state. *Faraday Discuss.* **2023**, *244*, 222–240.
- (58) Chadwick, F. M.; Krämer, T.; Gutmann, T.; Rees, N. H.; Thompson, A. L.; Edwards, A. J.; Buntkowsky, G.; Macgregor, S. A.; Weller, A. S. Selective C–H Activation at a Molecular Rhodium Sigma-Alkane Complex by Solid/Gas Single-Crystal to Single-Crystal H/D Exchange. *J. Am. Chem. Soc.* **2016**, *138*, 13369–13378.
- (59) McKay, A. I.; Bukvic, A. J.; Tegner, B. E.; Burnage, A. L.; Martínez-Martínez, A. J.; Rees, N. H.; Macgregor, S. A.; Weller, A. S. Room Temperature Acceptorless Alkane Dehydrogenation from Molecular  $\sigma$ -Alkane Complexes. *J. Am. Chem. Soc.* **2019**, *141*, 11700–11712.
- (60) Bukvic, A. J.; Burnage, A. L.; Tizzard, G. J.; Martínez-Martínez, A. J.; McKay, A. I.; Rees, N. H.; Tegner, B. E.; Krämer, T.; Fish, H.; Warren, M. R. A Series of Crystallographically Characterized Linear and Branched  $\sigma$ -Alkane Complexes of Rhodium: From Propane to 3-Methylpentane. *J. Am. Chem. Soc.* **2021**, *143*, 5106–5120.
- (61) Krämer, T.; Chadwick, F. M.; Macgregor, S. A.; Weller, A. S. Solid-State Confinement Effects in Selective exo-H/D Exchange in the Rhodium  $\sigma$ -Norbornane Complex  $[(\text{C}_7\text{PCH}_2\text{CH}_2\text{PC}_7\text{Y}_2)\text{Rh}(\eta^2, \eta^2\text{-C}_7\text{H}_{12})][\text{BAR}^{\text{F}}_4]$ . *Helv. Chim. Acta* **2023**, *106*, No. e202200154.
- (62) Doyle, L. R.; Thompson, E. A.; Burnage, A. L.; Whitwood, A. C.; Jenkins, H. T.; Macgregor, S. A.; Weller, A. S. MicroED characterization of a robust cationic  $\sigma$ -alkane complex stabilized by the  $[\text{B}(3,5\text{-}(\text{SF}_3)_2\text{C}_6\text{H}_3)_4]^-$  anion, via on-grid solid/gas single-crystal to single-crystal reactivity. *Dalton Trans.* **2022**, *51*, 3661–3665.
- (63) Martínez-Martínez, A. J.; Rees, N. H.; Weller, A. S. Reversible Encapsulation of Xenon and  $\text{CH}_2\text{Cl}_2$  in a Solid-State Molecular Organometallic Framework (Guest@SMOM). *Angew. Chem. Int. Ed.* **2019**, *58*, 16873–16877.
- (64) Altus, K. M.; Sajjad, M. A.; Gyton, M. R.; Whitwood, A. C.; Page, S. J.; Macgregor, S. A.; Weller, A. S. Solid/Gas In Crystallo Reactivity of an Ir(I) Methylidene Complex. *Organometallics* **2024**, *43*, 3137–3142.
- (65) We have recently shown that addition of excess  $\text{H}_2$  to  $[\text{Ir}(\text{Bu-PONOP})(=\text{CH}_2)][\text{BAR}^{\text{F}}_4]$  in a SC-SC transformation results in the loss of methane to ultimately form  $[\text{Ir}(\text{Bu-PONOP})\text{H}_2][\text{BAR}^{\text{F}}_4]$ , similar to solution-based reactivity. See ref 64 and references therein.
- (66) Kataoka, S.; Kitagawa, D.; Sotome, H.; Ito, S.; Miyasaka, H.; Bardeen, C. J.; Kobatake, S. Relationship between spatially heterogeneous reaction dynamics and photochemical kinetics in single crystals of anthracene derivatives. *Chem. Sci.* **2024**, *15*, 13421–13428.
- (67) Wang, C.-H.; Das, A.; Gao, W.-Y.; Powers, D. C. Probing Substrate Diffusion in Interstitial MOF Chemistry with Kinetic Isotope Effects. *Angew. Chem. Int. Ed.* **2018**, *57*, 3676–3681.
- (68) Iliescu, A.; Oppenheim, J. J.; Sun, C.; Dincă, M. Conceptual and Practical Aspects of Metal–Organic Frameworks for Solid–Gas Reactions. *Chem. Rev.* **2023**, *123*, 6197–6232.
- (69) Pike, S. D.; Krämer, T.; Rees, N. H.; Macgregor, S. A.; Weller, A. S. Stoichiometric and Catalytic Solid–Gas Reactivity of Rhodium Bis-phosphine Complexes. *Organometallics* **2015**, *34*, 1487–1497.
- (70) Andino, J. G.; Caulton, K. G. Mechanism of N/O Bond Scission of  $\text{N}_2\text{O}$  by an Unsaturated Rhodium Transient. *J. Am. Chem. Soc.* **2011**, *133*, 12576–12583.
- (71) Tsvetkov, N. P.; Laird, M. F.; Fan, H.; Pink, M.; Caulton, K. G. Surprising isomer preference on Ir(III), favoring facile H–C(sp<sup>3</sup>) bond cleavage. *Chem. Commun.* **2009**, 4578–4580.
- (72) Verat, A. Y.; Pink, M.; Fan, H.; Tomaszewski, J.; Caulton, K. G.  $[(\text{Bu}_2\text{PCH}_2\text{SiMe}_2)_2\text{N}]\text{RhI}$ ? Rapidly Reversible H–C(sp<sup>3</sup>) and H–

C(sp<sup>2</sup>) Bond Cleavage by Rhodium(I). *Organometallics* **2008**, *27*, 166–168.

(73) Biswas, S.; Blessent, M. J.; Gordon, B. M.; Zhou, T.; Malakar, S.; Wang, D. Y.; Krogh-Jespersen, K.; Goldman, A. S. Origin of Regioselectivity in the Dehydrogenation of Alkanes by Pincer–Iridium Complexes: A Combined Experimental and Computational Study. *ACS Catal.* **2021**, *11*, 12038–12051.

(74) Renkema, K. B.; Kissin, Y. V.; Goldman, A. S. Mechanism of Alkane Transfer-Dehydrogenation Catalyzed by a Pincer-Ligated Iridium Complex. *J. Am. Chem. Soc.* **2003**, *125*, 7770–7771.

(75) Adams, G. M.; Chadwick, F. M.; Pike, S. D.; Weller, A. S. A CH<sub>2</sub>Cl<sub>2</sub> complex of a [Rh(pincer)]<sup>+</sup> cation. *Dalton Trans.* **2015**, *44*, 6340–6342.

(76) Royle, C. G.; Sotorrios, L.; Gyton, M. R.; Brodie, C. N.; Burnage, A. L.; Furfari, S. K.; Marini, A.; Warren, M. R.; Macgregor, S. A.; Weller, A. S. Single-Crystal to Single-Crystal Addition of H<sub>2</sub> to [Ir(iPr-PONOP)(propene)][BAR<sup>F</sup><sub>4</sub>] and Comparison Between Solid-State and Solution Reactivity. *Organometallics* **2022**, *41*, 3270–3280.

(77) Goodall, J. C.; Sajjad, M. A.; Thompson, E. A.; Page, S. J.; Kerrigan, A. M.; Jenkins, H. T.; Lynam, J. M.; Macgregor, S. A.; Weller, A. S. In crystallo lattice adaptivity triggered by solid-gas reactions of cationic group 7 pincer complexes. *Chem. Commun.* **2023**, *59*, 10749–10752.

(78) Huang, Z.; White, P. S.; Brookhart, M. Ligand exchanges and selective catalytic hydrogenation in molecular single crystals. *Nature* **2010**, *465*, 598–601.

(79) Ozerov, O. V.; Guo, C.; Papkov, V. A.; Foxman, B. M. Facile Oxidative Addition of N–C and N–H Bonds to Monovalent Rhodium and Iridium. *J. Am. Chem. Soc.* **2004**, *126*, 4792–4793.

(80) Vitórica-Yrezábal, I. J.; Libri, S.; Loader, J. R.; Mínguez Espallargas, G.; Hippler, M.; Fletcher, A. J.; Thompson, S. P.; Warren, J. E.; Musumeci, D.; Ward, M. D.; et al. Coordination Polymer Flexibility Leads to Polymorphism and Enables a Crystalline Solid–Vapour Reaction: A Multi-technique Mechanistic Study. *Chem. - Eur. J.* **2015**, *21*, 8799–8811.

(81) Schumacher, C.; Crawford, D. E.; Raguž, B.; Glaum, R.; James, S. L.; Bolm, C.; Hernández, J. G. Mechanochemical dehydrocoupling of dimethylamine borane and hydrogenation reactions using Wilkinson's catalyst. *Chem. Commun.* **2018**, *54*, 8355–8358.

(82) Johnson, C. L.; Storm, D. J.; Sajjad, M. A.; Gyton, M. R.; Duckett, S. B.; Macgregor, S. A.; Weller, A. S.; Navarro, M.; Campos, J. A Gold(I)–Acetylene Complex Synthesised using Single-Crystal Reactivity. *Angew. Chem. Int. Ed.* **2024**, *63*, No. e202404264.

(83) Sato, O. Dynamic molecular crystals with switchable physical properties. *Nat. Chem.* **2016**, *8*, 644–656.

(84) Chapp, S. M.; Schley, N. D. Reversible C(sp<sup>3</sup>)-Si Oxidative Addition of Unsupported Organosilanes: Effects of Silicon Substituents on Kinetics and Thermodynamics. *J. Am. Chem. Soc.* **2021**, *143*, 5534–5539.

(85) McKay, A. I.; Martínez-Martínez, A. J.; Griffiths, H. J.; Rees, N. H.; Waters, J. B.; Weller, A. S.; Krämer, T.; Macgregor, S. A. Controlling Structure and Reactivity in Cationic Solid-State Molecular Organometallic Systems Using Anion Templating. *Organometallics* **2018**, *37*, 3524–3532.

(86) Hartwig, J. F.; De Gala, S. R. A Continuum Resulting from Equilibrium between Two Structural Extremes in Tungstenocene and Niobocene Boryl and Hydridoborate Complexes.  $\pi$ -Bonding in a d<sup>2</sup> Boryl System and the First d<sup>0</sup> Boryl Complex. *J. Am. Chem. Soc.* **1994**, *116*, 3661–3662.

(87) Zhang, W.; Moore, C. E.; Zhang, S. Multiple Proton-Coupled Electron Transfers at a Tricopper Cluster: Modeling the Reductive Regeneration Process in Multicopper Oxidases. *J. Am. Chem. Soc.* **2022**, *144*, 1709–1717.

(88) The small amount of 2[BAR<sup>F</sup><sub>4</sub>] observed in the recovered crystalline material, alongside other minor impurities, suggests an inverse isotope effect is operating in solution on recrystallization at –40 °C that results in accelerated loss of methane (CD<sub>4</sub>).

(89) Parkin, G. Temperature-Dependent Transitions Between Normal and Inverse Isotope Effects Pertaining to the Interaction of

H–H and C–H Bonds with Transition Metal Centers. *Acc. Chem. Res.* **2009**, *42*, 315–325.

(90) Bullock, R. M.; Bender, B. R.; Isotope Methods – Homogeneous. In *Encyclopedia of Catalysis*; John Wiley & Sons, 2002.

(91) Jones, W. D. Isotope Effects in C–H Bond Activation Reactions by Transition Metals. *Acc. Chem. Res.* **2003**, *36*, 140–146.

(92) Lantero, D. R.; Ward, D. L.; Smith, M. R. Group 5 Metallocene Complexes as Models for Metal-Mediated Hydroboration: Synthesis of a Reactive Borane Adduct, endo-Cp\*<sub>2</sub>Nb(H<sub>2</sub>BO<sub>2</sub>C<sub>6</sub>H<sub>4</sub>), via Hydroboration of Coordinated Olefins. *J. Am. Chem. Soc.* **1997**, *119*, 9699–9708.

(93) If this reaction is performed at 80 °C under an Ar atmosphere (1 bar at 298 K) in a sealed NMR tube, solution NMR spectroscopy (CD<sub>2</sub>Cl<sub>2</sub>, –80 °C) of the resulting material shows that 2[BAR<sup>F</sup><sub>4</sub>] is formed in 80% purity, alongside 1[BAR<sup>F</sup><sub>4</sub>] (~10%), [Ir(<sup>t</sup>Bu-PONOP)H<sub>2</sub>][BAR<sup>F</sup><sub>4</sub>] (~5%, ref.115) and the new Ir(I) dinitrogen complex [Ir(<sup>t</sup>Bu-PONOP)N<sub>2</sub>][BAR<sup>F</sup><sub>4</sub>], 3[BAR<sup>F</sup><sub>4</sub>] (5%). We thus propose that this complex forms from trace (1–2 ppm) levels of N<sub>2</sub> present in the argon. See, for example, ref 75.

(94) Albrecht, M. Cyclometalation Using d-Block Transition Metals: Fundamental Aspects and Recent Trends. *Chem. Rev.* **2010**, *110*, 576–623.

(95) Brookhart, M.; Green, M. L. H.; Parkin, G. Agostic interactions in transition metal compounds. *Proc. Nat. Acad. Sci.* **2007**, *104*, 6908–6914.

(96) Polukeev, A. V.; Kuklin, S. A.; Petrovskii, P. V.; Peregodov, A. S.; Dolgushin, F. M.; Ezernitskaya, M. G.; Koridze, A. A. Reactions of iridium bis(phosphinite) pincer complexes with protic acids. *Russ. Chem. Bull.* **2010**, *59*, 745–749.

(97) Mohammad, H. A. Y.; Grimm, J. C.; Eichele, K.; Mack, H.-G.; Speiser, B.; Novak, F.; Quintanilla, M. G.; Kaska, W. C.; Mayer, H. A. C–H Oxidative Addition with a (PCP)Ir(III)-Pincer Complex. *Organometallics* **2002**, *21*, 5775–5784.

(98) Polukeev, A. V.; Tasić, M. Oxidation-induced C–H bond activation in iridium pincer complexes. *Dalton Trans.* **2023**, *52*, 7701–7708.

(99) Smart, J. E.; Prokes, I.; Leforestier, B.; Chaplin, A. B. Rhodium(III) and Iridium(III) Complexes of a Neopentyl-substituted PNP Pincer Ligand that Feature Agostic Interactions. *Organometallics* **2024**, *43*, 1143–1154.

(100) Yano, T.; Moroe, Y.; Yamashita, M.; Nozaki, K. Neopentyl-substituted PNP-pincer Ligand: Complexation with Iridium to Form an Iridacycle via Alkyl C–H Activation. *Chem. Lett.* **2008**, *37*, 1300–1301.

(101) Bhatti, T. M.; Kumar, A.; Parihar, A.; Moncy, H. K.; Emge, T. J.; Waldie, K. M.; Hasanayn, F.; Goldman, A. S. Metal–Ligand Proton Tautomerism, Electron Transfer, and C(sp<sup>3</sup>)-H Activation by a 4-Pyridinyl-Pincer Iridium Hydride Complex. *J. Am. Chem. Soc.* **2023**, *145*, 18296–18306.

(102) See [Supporting Information](#).

(103) Phillips, N.; Rowles, J.; Kelly, M. J.; Riddlestone, I.; Rees, N. H.; Dervisi, A.; Fallis, I. A.; Aldridge, S. Sterically Encumbered Iridium Bis(N-heterocyclic carbene) Complexes: Air-Stable 14-Electron Cations and Facile Degenerate C–H Activation. *Organometallics* **2012**, *31*, 8075–8078.

(104) Paschai Darian, L. K.; Ballmann, J.; Gade, L. H. T-shaped 14 Electron Rhodium Complexes: Potential Active Species in C–H Activation. *Angew. Chem. Int. Ed.* **2024**, *63*, No. e202416814.

(105) Ghosh, R.; Kanzelberger, M.; Emge, T. J.; Hall, G. S.; Goldman, A. S. Dinitrogen Complexes of Pincer-Ligated Iridium. *Organometallics* **2006**, *25*, 5668–5671.

(106) Martínez-Martínez, A. J.; Royle, C. G.; Furfari, S. K.; Suriye, K.; Weller, A. S. Solid–State Molecular Organometallic Catalysis in Gas/Solid Flow (Flow-SMOM) as Demonstrated by Efficient Room Temperature and Pressure 1-Butene Isomerization. *ACS Catal.* **2020**, *10*, 1984–1992.

(107) The equivalent, non-cyclometallated, complex [Ir(<sup>t</sup>Bu-PONOP)(CO)MeH][BAR<sup>F</sup><sub>4</sub>] undergoes reductive elimination at 80 °C in 3 h (ClCH<sub>2</sub>CH<sub>2</sub>Cl solution) to form 3[BAR<sup>F</sup><sub>4</sub>]. See. ref.45.

(108) Crumpton-Bregel, D. M.; Goldberg, K. I. Mechanisms of C–C and C–H Alkane Reductive Eliminations from Octahedral Pt(IV): Reaction via Five-Coordinate Intermediates or Direct Elimination? *J. Am. Chem. Soc.* **2003**, *125*, 9442–9456.

(109) Cheng, C.; Kim, B. G.; Guironnet, D.; Brookhart, M.; Guan, C.; Wang, D. Y.; Krogh-Jespersen, K.; Goldman, A. S. Synthesis and Characterization of Carbazolide-Based Iridium PNP Pincer Complexes. Mechanistic and Computational Investigation of Alkene Hydrogenation: Evidence for an Ir(III)/Ir(V)/Ir(III) Catalytic Cycle. *J. Am. Chem. Soc.* **2014**, *136*, 6672–6683.

(110) Johnson, A.; Royle, C. G.; Brodie, C. N.; Martínez-Martínez, A. J.; Duckett, S. B.; Weller, A. S.  $\eta^2$ -Alkene Complexes of [Rh(PONOP-Pr)(L)]<sup>+</sup> Cations (L = COD, NBD, Ethene). Intramolecular Alkene-Assisted Hydrogenation and Dihydrogen Complex [Rh(PONOP-Pr)( $\eta$ -H<sub>2</sub>)]<sup>+</sup>. *Inorg. Chem.* **2021**, *60*, 13903–13912.

(111) Agueda, V. I.; Delgado, J. A.; Uguina, M. A.; Brea, P.; Spjelkavik, A. I.; Blom, R.; Grande, C. Adsorption and diffusion of H<sub>2</sub>, N<sub>2</sub>, CO, CH<sub>4</sub> and CO<sub>2</sub> in UTSA-16 metal-organic framework extrudates. *Chem. Eng. Sci.* **2015**, *124*, 159–169.

(112) Burada, P. S.; Hänggi, P.; Marchesoni, F.; Schmid, G.; Talkner, P. Diffusion in Confined Geometries. *ChemPhyschem* **2009**, *10*, 45–54.

(113) Abu-Hasanayn, F.; Krogh-Jespersen, K.; Goldman, A. S. Theoretical study of primary and secondary deuterium equilibrium isotope effects for hydrogen and methane addition to iridium complex trans-Ir(PR<sub>3</sub>)<sub>2</sub>(CO)X. *J. Am. Chem. Soc.* **1993**, *115*, 8019–8023.

(114) The @ nomenclature acknowledges the fact that in the calculations CH<sub>4</sub> loss from  $\alpha$ -[1][BAR<sup>F</sup><sub>4</sub>] is not the microscopic reverse of CH<sub>4</sub> addition to [2][BAR<sup>F</sup><sub>4</sub>]. The former gives a single [2]<sup>+</sup> cation within the  $\alpha$ -[1][BAR<sup>F</sup><sub>4</sub>] unit cell (i.e. 2<sup>+</sup>@ $\alpha$ -[1][BAR<sup>F</sup><sub>4</sub>]) whereas the latter gives a single [1]<sup>+</sup> cation within the [2][BAR<sup>F</sup><sub>4</sub>] unit cell (i.e. 1<sup>+</sup>@[2][BAR<sup>F</sup><sub>4</sub>]).

(115) Doyle, L. R.; Galpin, M. R.; Furfari, S. K.; Tegner, B. E.; Martínez-Martínez, A. J.; Whitwood, A. C.; Hicks, S. A.; Lloyd-Jones, G. C.; Macgregor, S. A.; Weller, A. S. Inverse Isotope Effects in Single-Crystal to Single-Crystal Reactivity and the Isolation of a Rhodium Cyclooctane  $\sigma$ -Alkane Complex. *Organometallics* **2022**, *41*, 284–292.

(116) Findlater, M.; Schultz, K. M.; Bernskoetter, W. H.; Cartwright-Sykes, A.; Heinekey, D. M.; Brookhart, M. Dihydrogen Complexes of Iridium and Rhodium. *Inorg. Chem.* **2012**, *51*, 4672–4678.

(117) Beckett, G.; Beech-Brandt, J.; Leach, K.; Payne, Z.; Simpson, A.; Smith, L.; Turner, A.; Whiting, A. ARCHER2 Service Description. *Zenodo* 2024, <https://doi.org/10.5281/zenodo.14507040>.